Strontium Isotope Fractionation of Planktic Foraminifera and Inorganic Calcite

Florian Böhm, Anton Eisenhauer, Jianwu Tang, Martin Dietzel, Andre Krabbenhöft,

Basak Kisakürek, Christian Horn

Preprint

Strontium isotope fractionation of planktic foraminifera and inorganic calcite

Florian Böhm[1], Anton Eisenhauer[1], Jianwu Tang[2], Martin Dietzel[3], Andre Krabbenhöft[1], Basak Kisakürek[1], Christian Horn[1]

1: IFM-GEOMAR, Leibniz Institute for Marine Sciences, Kiel, Germany
2: Department of Earth & Environmental Sciences, Tulane University, New Orleans, USA
3: Institute of Applied Geosciences, Graz University of Technology, Graz, Austria

Abstract

We have investigated the strontium isotope fractionation ($\Delta^{88/86}Sr_{carb-aq}$) between inorganic calcite and aqueous Sr^{2+} ions by precipitation experiments at a constant temperature of 25°C and precipitation rates (R) ranging from $10^{2.3}$ to $10^{4.2}$ µmol/m²/h. Strontium isotope ratios were measured using the ^{87}Sr-^{84}Sr double spike technique. It was found that strontium isotope fractionation in these calcites is strongly dependent on the precipitation rate:

$$\Delta^{88/86}Sr_{carb-aq} = -0.08 * \log(R\ [\text{µmol/m}^2/\text{h}]) + 0.08$$

The measured $\delta^{88/86}Sr$ values are significantly correlated with previously measured $\delta^{44/40}Ca$ and Sr/Ca values of the same calcite samples:

$$\Delta^{88/86}Sr_{carb-aq} = +0.18 * \Delta^{44/40}Ca_{carb-aq} - 0.01$$

$$\Delta^{88/86}Sr_{carb-aq} = -1.5 * K_d^{Sr} - 0.03$$

The slope of $^{88}Sr/^{86}Sr$ versus $^{44}Ca/^{40}Ca$ fractionation is 0.18 ± 0.04 and compatible with a kinetic fractionation during dehydration of the strontium and calcium ions, but not with isotope fractionation in a diffusive boundary layer. Using published equilibrium $\Delta^{44/40}Ca_{carb-aq}$ and K_d^{Sr} values we estimate the equilibrium isotope fractionation of strontium to be very close to zero ($\Delta^{88/86}Sr_{eq(carb-aq)} = -0.01 \pm 0.06‰$). This estimate is confirmed by strontium isotope values of natural inorganic calcites that precipitated very slowly in basalts of the ocean crust.

The results from the inorganic calcites are used to explain strontium isotope fractionation of planktic foraminifera. Specimens of two warm water species (*Globigerinoides ruber* and *Globigerinoides sacculifer*) were picked from the Holocene section of a Caribbean sediment core. We found no significant difference in $\delta^{88/86}Sr$ between the two species. In addition, *G. ruber* specimens from Marine Isotope Stage 2 in the same core show $\delta^{88/86}Sr$ values identical to the Holocene specimens.

The strontium isotopes of both foraminifera species are strongly fractionated ($\Delta^{88/86}Sr_{carb-aq}$ = -0.248 ± 0.005‰) when compared to published data of other major marine calcifiers. Applying the results from the inorganic precipitation experiments we find that the strong foraminiferal strontium isotope fractionation can be explained by calcification in a largely open system at high precipitation rates, comparable in magnitude to rates known from scleractinian reef corals. This interpretation is in good agreement with the kinetic calcification model for planktic foraminifera by Kisakürek et al. (*GCA* **75** (2011), 427), which was based on calcium isotopes and elemental Sr/Ca ratios.

Keywords: inorganic calcite, planktic foraminifera, stable strontium isotopes, calcium isotopes, precipitation rate, diffusive boundary layer, isotope fractionation.

1. INTRODUCTION

Planktic foraminifera are among the most important calcium carbonate ($CaCO_3$) producers in the modern oceans, responsible for about 20% of the global $CaCO_3$ accumulation flux. Thus, they play an important role in the marine calcium cycle (Milliman and Droxler, 1996; Schiebel, 2002). Strontium and calcium cycling are closely coupled in the marine environment. With an average strontium concentration of about 1300 μg/g (Carpenter and Lohman, 1992) planktic foraminiferal calcite also represents an important strontium sink, responsible for about 5-10% of the marine strontium burial flux (Krabbenhöft et al., 2010).

Recent compilations of the marine strontium isotope budget show that several major $CaCO_3$ producers (reef corals, *Halimeda*, coccoliths, molluscs) have $\Delta^{88/86}Sr_{carb-aq}$ values between -0.2 and -0.1‰, while planktic foraminifera have a significantly lower $\Delta^{88/86}Sr_{carb-aq}$ value of about -0.25‰ or even less (Krabbenhöft et al., 2010; Liebetrau et al., 2009; Stevenson et al., 2010; $\Delta^{88/86}Sr_{carb-aq}$ = $\delta^{88/86}Sr_{sample}$ - $\delta^{88/86}Sr_{fluid}$, $\delta^{88/86}Sr$ = [$(^{88}Sr/^{86}Sr)_{sample}$ / $(^{88}Sr/^{86}Sr)_{standard}$ - 1] * 1000). Therefore shells of planktic foraminifera may constitute a significant sink of isotopically light strontium in the global strontium cycle.

Little is known about fractionation mechanisms of strontium isotopes during mineral formation. The recent developments in the precision of strontium isotope fractionation analysis (Fietzke and Eisenhauer, 2006; Ohno and Hirata, 2007; Krabbenhöft et al., 2009) have provided data for the first overviews of the strontium isotope systematics in marine biogenic carbonates and for continental weathering (Halicz et al., 2008; Rüggeberg et al., 2008; de Souza et al., 2010; Krabbenhöft et al.,

2010). However, systematic investigations of strontium isotope fractionation during mineral formation are still very rare (Fietzke and Eisenhauer, 2006; Halicz et al., 2008).

On the other hand, investigations of calcium isotopes in experimentally precipitated and diagenetically altered calcite have provided evidence for very strong precipitation rate effects on isotope fractionation (Lemarchand et al., 2004; Fantle and DePaolo, 2007; Tang et al., 2008b). In order to find out whether similar kinetic effects also control strontium isotope fractionation, we investigated inorganic calcite samples that were precipitated in experiments with a given range of distinct precipitation rates at constant temperature. The same samples were previously studied for elemental strontium partitioning and calcium isotope fractionation (Tang et al., 2008 a, b). Results from these two studies showed an inverse linear correlation between strontium partitioning ($K_d^{Sr} = (Sr/Ca)_{calcite} / (Sr/Ca)_{fluid}$) and calcium isotope fractionation ($\Delta^{44/40}Ca_{carb-aq} = \delta^{44/40}Ca_{calcite} - \delta^{44/40}Ca_{fluid}$), which are both mainly controlled by precipitation rate. Based on these results, planktic foraminifera data were interpreted by Kisakürek et al. (2011) to indicate calcification at high rates in a semi-open system, with less than half of the available calcium being utilized for calcite precipitation.

In this study, we measured the strontium isotopic composition ($\delta^{88/86}Sr$) of inorganic calcite and of two species of planktic foraminifera, *Globigerinoides ruber* and *Globigerinoides sacculifer*, to test two hypotheses: 1. whether strontium isotope fractionation in calcite depends on precipitation rate, and 2. whether the relatively strong strontium isotope fractionation of planktic foraminiferal calcite is caused by high calcification rates.

2. MATERIAL AND METHODS

2.1. Foraminifera

Piston core SO 164-03-4 was collected from 2745 mbsl (meters below sea level) at the Beata Ridge in the Central Caribbean (16°32.37'N, 72°12.31'W) during the Sonne cruise SO164 in May 2002. Planktic foraminifera of the species *Globigerinoides sacculifer* and *Globigerinoides ruber* were picked from soft sediments in the upper 1.2 m of the core, consisting of sandy clay (Nürnberg et al., 2003). The sampled Holocene interval, 10-43 cm, corresponds to an age from about 1 to 7 ka (based on unpublished oxygen isotope data measured on benthic foraminifera, *Cibicidoides wuellerstorfi*, by Joachim Schönfeld, IFM-GEOMAR, Kiel). In addition we measured *G. ruber* specimens from about 1 m depth, corresponding to Marine Isotope Stage 2 (last glacial maximum), about 22-25 ka. The glacial specimens formed at a lower temperature than the Holocene specimens and were used to check for a possible temperature dependence of foraminiferal strontium isotope fractionation. For

each strontium isotope analysis 50 to 80 specimens were picked from the 315 - 355 µm size fraction, corresponding to a sample weight of about 1 mg. Sediment samples were freeze dried, washed and sieved (>63 µm) before picking. The foraminifera were crushed, ultrasonically treated for 30 s and washed with water several times. Subsequently they were washed twice with methanol and rinsed with water, in order to remove any remaining clay particles. The washed samples were treated with a NaOH buffered H_2O_2 solution and heated to about 95 °C for 20 minutes. Finally, the samples were washed twice with water, dried, and dissolved in doubly distilled ca. 1.5 N HNO_3. The solutions were evaporated under infrared light and redissolved in 200 µl of 8 N HNO_3.

2.2. Inorganic calcite

Inorganic calcite samples were available from a previous study of strontium incorporation and calcium isotope fractionation described in Tang et al. (2008 a, b). In these experiments calcite was precipitated spontaneously using an advanced CO_2-diffusion technique adapted from Dietzel and Usdowski (1996) and Dietzel et al. (2004). This technique allows to simultaneously control precipitation rate and temperature.

Briefly, various precipitation rates were adjusted by the CO_2 flux through a polyethylene membrane at a constant temperature of 25°C. $SrCl_2 \cdot 6H_2O$ (Merck *pro analysi*) was added to 5 L of a $CaCl_2$-NH_4Cl solution (10 mM $CaCl_2$, 5 mM NH_4Cl) with an ionic strength of about 0.035 M. The molar Sr/Ca ratio in solution was about 0.01. Less than 2% of the strontium in solution was precipitated during the experiments. The pH was kept constant during precipitation at 8.3 by pH-stat titration with a NaOH solution. Precipitation rates were calculated from the total amount of calcite precipitated, the time period of calcite growth, and the average crystal surface area for each experimental run (Tang et al., 2008a).

Six samples from these experiments were selected for strontium isotope analyses (Table 1) to cover the whole available range of precipitation rates. From each of the 6 experiments between 1 and 7 mg of calcite were dissolved in ca. 1.5 N HNO_3, dried down and redissolved in 8 N HNO_3.

2.3. Natural calcite cements

Two samples of inorganic calcite precipitated in veins during low temperature alteration of ocean crust basalt were picked from cores drilled during DSDP Leg 37 (Mid-Atlantic Ridge, 37°N, water depth 3188 m). Two samples were collected from centimetre-sized veins, using a hand-held microdrill. Several mg of calcite powders were collected for each sample, dissolved in ca. 1.5 N

HNO_3, dried down and redissolved in 8 N HNO_3.

The basalts at this site formed during geomagnetic polarity chron C5r (11 to 12 Ma, Miles and Howe, 1977; Gradstein et al., 2004). The calcites precipitated slightly later, at about 7 Ma, as evident from the radiogenic $^{87}Sr/^{86}$ ratios of the samples (Table 2). Oxygen isotope values of the two samples indicate formation in deep water at temperatures of about 2°C. Due to the limited supply of carbonate ions in the cold deep water, these calcite cements presumably grew with very slow precipitation rates and show quasi-equilibrium values for calcium isotopes (Böhm et al., 2009). Using the rate dependence of K_d^{Sr} from Tang et al (2008a) and measured Sr/Ca ratios of the calcite samples (Table 2) we can roughly estimate the precipitation rate of the vein calcites to be in the order of 10 $\mu mol/m^2/h$. This value is calculated adopting the modern seawater Sr/Ca of 8.6 mmol/mol in North Atlantic deep waters (deVilliers, 1999). If seawater Sr/Ca at 7 Ma was lower than in the modern oceans (about 7 mmol/mol, Coggon et al., 2010) then precipitation rates would have been slightly higher, corresponding to about 30 $\mu mol/m^2/h$. In both cases calcium isotopes would be close to equilibrium ($\Delta^{44/40}Ca_{carb-aq}$ of approximately -0.3‰ or -0.4‰, respectively, Tang et al., 2008b).

2.4. Strontium isotope analysis

Strontium isotope fractionation ($\delta^{88/86}Sr$) as well as radiogenic strontium ($^{87}Sr/^{86}Sr$) were measured on aliquots of each sample, following the procedure described in Krabbenhöft et al. (2009). Measurements were carried out at the IFM-GEOMAR mass spectrometer facilities in Kiel, Germany, with a Finnigan (ThermoFisher) Triton TI (Thermal Ionization Mass Spectrometer, TIMS). Samples containing 560 to 2400 ng of strontium were split into two aliquots. One aliquot was spiked with a $^{87}Sr/^{84}Sr$ double spike to measure $\delta^{88/86}Sr$, with about 95% of ^{84}Sr contributed by the spike to the total ^{84}Sr in the spike-sample mixture (Krabbenhöft et al., 2009). Strontium of spiked and unspiked sample aliquots was extracted from the sample matrix with a chromatographic column setup, using 200 to 300 μl of Eichrom SrSpec resin for samples with 280 to 1200 ng strontium. Samples were loaded and washed with 8N HNO_3. Strontium was eluted with 6 ml ultrapure H_2O (18.2 MΩ*cm at 25°C). After separation samples were dried down in teflon beakers and boiled at 120°C for several hours with a 1:1 mixture of HNO_3 (65%) and H_2O_2 (30%) to remove residual resin. Finally samples were dried again and 140 to 600 ng of strontium were loaded with H_3PO_4 and $TaCl_5$ activator onto Re filaments. No column chemistry was carried out for preparation of the standard (NIST SRM 987) and for the $SrCl_2$ used in the calcite precipitation setups.

Measurements were made with single filaments at a temperature of about 1350-1400°C and a typical ^{88}Sr signal intensity of about 50 pA corresponding to a voltage of 5V. Signals of masses 84 to 88 were recorded simultaneously. Mass 85 was used to correct for ^{87}Rb interferences, assuming a natural ^{87}Rb/^{85}Rb ratio of 0.3857.

Spike correction and normalization of the results was carried out as described in Krabbenhöft et al. (2009). Radiogenic ^{87}Sr/^{86}Sr ratios were determined by normalizing the spike corrected ^{87}Sr/^{86}Sr* ratios (for definition see Appendix A in Krabbenhöft et al., 2010) to the recommended ^{86}Sr/^{88}Sr ratio of 0.1194 (Nier, 1938, Steiger and Jäger, 1977). The standard NIST SRM987 was measured with an average ^{87}Sr/^{86}Sr value of 0.710233(8) (1 sd, n = 12). Radiogenic ^{87}Sr/^{86}Sr ratios of all natural samples were adjusted to a ^{87}Sr/^{86}Sr$_{SRM987}$ of 0.710248 for comparison with values of the "Strontium Isotope Stratigraphy" of McArthur and Howarth (2004).

The ^{88}Sr/^{86}Sr ratios are reported in the common delta notation relative to NIST SRM987: $\delta^{88/86}$Sr = [(^{88}Sr/^{86}Sr)$_{sample}$ / (^{88}Sr/^{86}Sr)$_{SRM987}$ - 1] * 1000 using the ^{88}Sr/^{86}Sr ratio of SRM987 standards measured during the same session as the samples. The isotope fractionation is given as $\Delta^{88/86}$Sr$_{carb-aq}$ = $\delta^{88/86}$Sr$_{calcite}$ - $\delta^{88/86}$Sr$_{fluid}$. Errors are based on repeated analyses of samples and standards and are given as 2SEM (standard error of the mean), unless noted otherwise. The average ^{88}Sr/^{86}Sr ratio of SRM987 was determined as 8.37515(14). The long-term analytical precision for $\delta^{88/86}$Sr was determined from repeated measurements of SRM987 as ±0.01‰ (1sd, n = 12).

Two batches of SrCl$_2$ were used in the calcite precipitation experiments, showing different ^{87}Sr/^{86}Sr ratios [0.70784(2) and 0.70869(1)] but similar $\delta^{88/86}$Sr values (0.158±0.006‰, n=7, and 0.154±0.009‰, n=5). We therefore pooled all measured $\delta^{88/86}$Sr values of the two batches, resulting in an average $\delta^{88/86}$Sr of 0.156±0.005‰ (2 SEM, n = 12). This value was adopted for the strontium isotopic composition of the fluids used in all precipitation experiments.

With only up to 2% of the dissolved strontium used in the experiments, the influence of Rayleigh fractionation effects is insignificant (<0.002‰ for bulk calcite samples). Up to 15% of the calcium in solution was taken up by the precipitated calcite introducing a small systematic bias of up to 0.09‰ to the $\Delta^{44/40}$Ca$_{carb-aq}$ values. Calcium isotope values were therefore Rayleigh fractionation corrected based on data from Tang et al. (2008b) (Table 1). The strontium distribution coefficients (K$_d$^{Sr}) listed in Table 1 were corrected for Rayleigh distillation effects by Tang et al. (2008a).

3. RESULTS

The results of the strontium isotope analyses are shown in Tables 1, 2, and 3. The average

radiogenic $^{87}Sr/^{86}Sr$ ratios of Holocene *G. ruber*, glacial *G. ruber*, and Holocene *G. sacculifer* are 0.709176(5), 0.709173(4) and 0.709167(10), respectively. The values are indistinguishable within error (p = 0.25, t-test). They are identical within statistical uncertainty to the average $^{87}Sr/^{86}Sr$ ratio of modern seawater calculated from three recent publications (0.709175(8), McArthur et al., 2006, Fantle and DePaolo, 2006, Krabbenhöft et al., 2009, $p_{ruber} = 0.80$, $p_{sacculifer} = 0.34$, t-test) indicating the preservation of a pristine seawater signal in the sampled foraminiferal calcite.

The average $\Delta^{88/86}Sr_{carb-aq}$ values of Holocene *G. ruber* (-0.25 ± 0.01‰), glacial *G. ruber* (-0.25 ± 0.01‰), and Holocene *G. sacculifer* (-0.25 ± 0.01‰) are indistinguishable within error ($p_{ruber-sacculifer}$ = 0.81, $p_{Holocene-glacial}$ = 0.30, t-test). There is no significant temperature influence on the $\Delta^{88/86}Sr_{carb-aq}$ values in the Holocene-glacial *G. ruber* data (R^2 = 0.28, p = 0.27, linear regression).

Strontium isotope fractionation ($\Delta^{88/86}Sr_{carb-aq}$) during the experimental calcite formation is significantly influenced by precipitation rate (Fig. 1). The resulting regression equation (with 95% confidence intervals) is:

$$\Delta^{88/86}Sr_{carb-aq} \text{ [‰]} = (-0.084 \pm 0.044) * \log(R[\mu mol/m^2/h]) + 0.08 \pm 0.15; (R^2 = 0.87, p = 0.003) \quad (1)$$

Comparison with the strontium distribution coefficient (K_d^{Sr}) measured on aliquots of the analyzed samples shows a significant negative correlation between $\Delta^{88/86}Sr_{carb-aq}$ and K_d^{Sr} (Fig. 2):

$$\Delta^{88/86}Sr_{carb-aq} \text{ [‰]} = (-1.50 \pm 0.7) * K_d^{Sr} - 0.03 \pm 0.09; (R^2 = 0.89, p = 0.002) \quad (2)$$

Assuming that the equilibrium K_d^{Sr} of calcite is close to zero (Tesoriero and Pankow, 1996, Tang et al. 2008a) we can use y-axis intercept of the regression equation (Eq. 2) to estimate the equilibrium fractionation of strontium isotopes for calcite to be $\Delta^{88/86}Sr_{eq(carb-aq)}$ = -0.03 ± 0.09‰. The two analyzed natural calcite samples show $\Delta^{88/86}Sr_{carb-aq}$ values in this range (Fig. 2).

Calcium isotope fractionation was previously measured on aliquots of the analyzed samples (Tang et al., 2008b). A regression between strontium isotopes and calcium isotopes shows a highly significant positive correlation (Fig. 3):

$$\Delta^{88/86}Sr_{carb-aq} \text{ [‰]} = (0.176 \pm 0.04) * \Delta^{44/40}Ca_{carb-aq} \text{ [‰]} - 0.01 \pm 0.05; (R^2 = 0.97, p = 0.0001) \quad (3)$$

The natural calcites fit very well on this regression (Fig. 3). Again we can estimate $\Delta^{88/86}Sr_{eq(carb-aq)}$ from the regression intercept, assuming $\Delta^{44/40}Ca_{eq(carb-aq)}$ = 0.0‰ (Fantle and DePaolo, 2007):

$\Delta^{88/86}Sr_{eq(carb-aq)} = -0.01 \pm 0.05‰$. Both estimates, based on K_d^{Sr} and $\Delta^{44/40}Ca_{carb-aq}$, agree within uncertainties and show an equilibrium strontium isotope fractionation ($\Delta^{88/86}Sr_{eq(carb-aq)}$) very close to zero.

4. DISCUSSION

4.1. Inorganic calcite

Our results show a significant rate dependence for strontium isotope fractionation in calcite. We observe increasing discrimination of heavy strontium isotopes with increasing precipitation rates (Fig. 1). In this regard strontium isotopes behave like calcium isotopes, which also show a negative correlation between precipitation rate and isotope fractionation (Tang et al., 2008b). The precipitation rate effect on calcium isotopes has been explained by two alternative models, both based on the interplay of kinetic and equilibrium isotope fractionations.

In the "surface entrapment model" (Watson, 2004; Tang et al., 2008a, b) kinetic fractionation leads to a preferential incorporation of light isotopes at the crystal surface. Subsequently, isotopic equilibrium is slowly approached through ion diffusion in the near surface region of the growing crystal. The isotopic equilibration of the former surface layer is eventually stopped when it is trapped under further crystal layers and diffusional ion exchange with the fluid is halted. The higher the precipitation rate the shorter is the time available for isotopic equilibration.

In the "surface reaction kinetic model" (DePaolo, 2011) kinetic fractionation during precipitation again leads to an enrichment of light isotopes in the crystal surface layer. Isotopic equilibration is approached by ion exchange between fluid and crystal surface, i.e. by precipitation/dissolution (forward/backward) reactions. Eqilibration is halted when due to continued growth the crystal layer is no longer in contact with the fluid.

In both models the isotopic composition of the crystal reflects equilibrium fractionation at slow precipitation rates and kinetic fractionation when crystal growth is fast. Both models can explain the interdependencies of rate and temperature controls of calcium isotopes as well as the Sr/Ca ratios observed in calcite (Tang et al., 2008a, b). By analogy with the calcium isotopes the two models can also be used to explain the rate dependence of strontium isotopes in the inorganic calcite samples. Two major factors control the isotopic rate effect of cation incorporation in a growing crystal: (1) the isotopic difference between the kinetically fractionated surface layer and the equilibrium composition; (2) the rate of isotopic equilibration of the crystal surface layer. The latter depends on

8

the cation diffusivity in the near surface layer of the crystal (surface entrapment model) or on the ratio between net precipitation rate and dissolution rate (surface reaction kinetic model). From this point of view comparing the rate dependencies of calcium and strontium isotopes may provide clues to the fractionation mechanism that leads to the isotopic enrichment of the surface layer.

It is well known that calcite crystals preferentially take up light calcium isotopes, with fractionation ($\Delta^{44/40}Ca_{carb-aq}$) commonly between -0.5 and -1.0‰, approaching -1.5‰ in some cases (e.g. Marriott et al., 2004; Lemarchand et al., 2004; DePaolo, 2004; Gussone et al., 2003, 2005, 2007). Equivalent preferential uptake of light strontium isotopes has been observed in several studies of calcite and aragonite (Fietzke and Eisenhauer, 2006; Ohno and Hirata, 2007; Halicz et al., 2008; Rüggeberg et al., 2008; Krabbenhöft et al., 2010; Knudson et al., 2010) and is also evident from the results of this study (Fig. 2).

On the other hand, it has been shown that the calcium isotopic compositions of calcite and ambient pore fluids are very similar ($\Delta^{44/40}Ca_{eq(carb-aq)} \approx 0.0$‰) in systems where sufficient time is available for isotopic equilibration (Fantle and DePaolo, 2007; Jacobson and Holmden, 2008; Böhm et al., 2009). This seems to be the case for strontium isotopes too ($\Delta^{88/86}Sr_{eq(carb-aq)} \approx 0.0$‰, Fig. 1). Therefore, in accord with the two rate models described above, the discrimination of heavy calcium and strontium isotopes during crystal formation is most likely a process occurring at the surface of the crystal under non-equilibrium conditions. It is caused by kinetic isotope fractionation ($\Delta^{44/40}Ca_{kin(carb-aq)} < -1.5$‰; $\Delta^{88/86}Sr_{kin(carb-aq)} < -0.3$‰). Equilibrium fractionation of calcite does not partition isotopes of either element ($\Delta^{44/40}Ca_{eq(carb-aq)} \approx 0$‰; $\Delta^{88/86}Sr_{eq(carb-aq)} \approx 0$‰). Consequently, the observed correlation of the rate dependent calcium and strontium isotope fractionations and the slope of the resulting regression line (Eq. 3, Fig. 3) should primarily reflect the ratio (β) of the respective $\Delta_{kin(carb-aq)}$ values of the two elements:

$$\Delta^{88/86}Sr_{kin(carb-aq)} = \beta * \Delta^{44/40}Ca_{kin(carb-aq)} \text{ or } \beta = \Delta^{88/86}Sr_{kin(carb-aq)} / \Delta^{44/40}Ca_{kin(carb-aq)} \qquad (4)$$

Eq. (4) can be interpreted to reflect the different masses of strontium and calcium with the assumption that the two elements differ in their reduced partition function ratios and reaction rate constant ratios only due to their different masses. This approach is certainly a crude approximation but, with the similar chemical behaviour of the two elements, may nevertheless provide some information about the possible frationation mechanisms that lead to the observed linear correlation of $\Delta^{88/86}Sr_{carb-aq}$ and $\Delta^{44/40}Ca_{carb-aq}$.

Eq. (4) can be derived from Eq. (5), the general equation for the mass dependence of isotope

fractionation (Young et al., 2002)

$$^{88/86}\alpha_{kin(carb\text{-}aq)} = {}^{44/40}\alpha_{kin(carb\text{-}aq)}{}^{\beta} \text{ or } \ln\left({}^{88/86}\alpha_{kin(carb\text{-}aq)}\right) = \beta * \ln\left({}^{44/40}\alpha_{kin(carb\text{-}aq)}\right) \qquad (5)$$

by recasting with $\Delta_{carb\text{-}aq} \approx 1000 \ln(\alpha_{carb\text{-}aq})$. The exponent β in Eq. (5) is a function of the respective isotope masses and the fractionation mechanism (Young et al., 2002)

$$\beta_{eq} = (87.906^{-1} - 85.909^{-1}) / (43.955^{-1} - 39.963^{-1}) = 0.12 \qquad (6)$$

$$\beta_{kin} = \log(\mu_{Sr(h)} / \mu_{Sr(l)}) / \log(\mu_{Ca(h)} / \mu_{Ca(l)}) \qquad (7a)$$

$$\beta_{diff} = \log(87.906 / 85.909) / \log(43.955 / 39.963) = 0.24 \qquad (7b)$$

for equilibrium, chemical kinetic, and diffusional kinetic fractionation mechanisms, respectively. The masses in Eqs. (6) and (7b) are the atomic masses of the strontium and calcium isotopes of interest. Masses in Eq. (7a), $\mu_{i(h)}$ and $\mu_{i(l)}$, represent reduced masses for the heavy and light isotopes of element i, respectively, where $\mu_i = M * m_i / (M + m_i)$. Symbol m_i denotes the atomic isotope mass of interest, M is the mass of the molecules contributing to the reacting complex bonded to the element of interest (Young et al., 2002).

The resultant value for equilibrium fractionation (Eq. 6) is $\beta_{eq} = 0.12$, calculated with the atomic masses of calcium and strontium. This is significantly lower than the measured value of 0.18 ± 0.04 (Eq. 3). However, the observed value is close to $\beta_{kin} = 0.19\pm0.04$ for chemical kinetic isotope fractionation during dehydration of Sr^{2+} and Ca^{2+} aquocomplexes, having 6 to 8 water molecules in the inner hydration sphere (Megyes et al., 2004; Seward et al., 1999; Tofteberg et al., 2006). The latter range of β_{kin} values is calculated with Eq. (7) by adopting the reduced masses of the aquocomplexes calculated with M = 108.1 amu for $(H_2O)_6$, M = 144.1 amu for $(H_2O)_8$ and the respective atomic strontium and calcium isotope masses.

Alternatively, kinetic fractionation during aqueous cation diffusion through a diffusive boundary layer (see Section 4.2) may explain the observed slope β. It was recently suggested that the atomic masses determine the fractionation of ions diffusing in water. The fractionation factor is further controlled by the residence time (τ_s) of water molecules in the inner solvation shell of the diffusing cation-aquocomplexes (Bourg et al., 2010). Assuming that Sr^{2+} and Ca^{2+} have similar τ_s (Kerisit and Parker, 2004) we can calculate $\beta_{diff} = 0.24$ with Eq. (7b). This value is significantly higher than the observed β of 0.18 ± 0.04. In addition, as will be shown in the next section, the isotope fractionation effects of cation diffusion in water are much too small to explain the observed isotope fractionation

of calcium and probably also of strontium.

We therefore suggest that chemical kinetic isotope fractionation (Bigeleisen, 1949) involving dehydration of Sr^{2+} and Ca^{2+} ions could be the primary mechanism responsible for the enrichment of light calcium and strontium isotopes in calcite crystals. Sr^{2+} and Ca^{2+} ions in aqueous solution obviously have to be dehydrated before they can be incorporated into the calcite crystal lattice (e.g. Raiteri et al., 2010; Marriott et al., 2004). This process can cause a kinetic isotope fractionation with a preferential dehydration of the lighter isotopes, which then could be more readily incorporated in the crystal lattice (DePaolo, 2011). This kinetic isotope partitioning can be temperature dependent, with decreasing partitioning at higher temperatures, because it involves the breaking of bonds (Bigeleisen, 1949). This temperature dependence of the dehydration induced kinetic isotope fractionation could explain the similar temperature control on the calcium isotopic composition of aragonite, calcite, and possibly calcium passing through biological membranes, which was observed in several previous studies (Gussone et al., 2003, 2005, 2006; Marriott et al., 2004; Böhm et al., 2006; Griffith et al., 2008b; Tang et al., 2008b).

As shown above the $\Delta^{88/86}Sr_{kin(carb-aq)}/\Delta^{44/40}Ca_{kin(carb-aq)}$ ratio observed in our data (Fig. 3, Eq. 3) can be explained by mass-dependent isotope fractionation. However, it is likely that differences in the chemical behaviour of the two elements additionally influence and modify the $\Delta^{88/86}Sr_{kin(carb-aq)}/\Delta^{44/40}Ca_{kin(carb-aq)}$ ratio. Nevertheless, the agreement between the observed slope (0.18±0.04) and the $\Delta^{88/86}Sr_{kin(carb-aq)}/\Delta^{44/40}Ca_{kin(carb-aq)}$ ratio expected for mass-dependent kinetic isotope fractionation (0.19±0.04) is in line with chemical kinetic isotope fractionation being the dominant mechanism responsible for the observed correlated rate effects.

Chemical kinetic isotope fractionation has previously been proposed to play a dominant role for the partitioning of magnesium and calcium isotopes during calcite precipitation (e.g. Gussone et al., 2003; DePaolo, 2011; Wombacher et al., 2011). Our results indicate that the same fractionation process may also control strontium isotope incorporation into calcite.

4.2. Diffusive boundary layer

It has been suggested that significant calcium and strontium isotope fractionation may occur in the diffusive boundary layer that forms around growing crystals and living organisms (Fantle and DePaolo, 2007; Watson and Müller, 2009). Diffusive boundary layers (DBL) form due to the depletion of the fluid in elements or isotopes that are preferentially taken up by the crystal or

organism. This selective uptake leads to the formation of gradients between the surface of the particle and the bulk solution (Zeebe and Wolf-Gladrow, 2001). Gradients in the concentrations of O_2, CO_2, CO_3^{2-}, H^+ and Ca^{2+} have been observed in water around living symbiotic foraminifera (e.g. Köhler-Rink and Kühl, 2005; de Beer et al., 2008) and at the surface of corals (Al-Horani et al., 2003). The maximum thickness of these boundary layers is determined by micro eddies in turbulent water (about 1 mm in ocean water), or is in the same order of magnitude as the particle radius (Zeebe and Wolf-Gladrow, 2001). In stirred solutions like in our experimental setup the boundary layer thickness can as small as 20 µm (DePaolo, 2011). Köhler-Rink and Kühl (2005) observed a decrease in $[Ca^{2+}]$ of about 5% between bulk solution and the surface of a shell of a calcifying planktic foraminifer. They calculated a diffusional transit time for Ca^{2+} ions through a 0.4 mm thick layer of about 4 minutes. Based on these observations it is plausible that calcium or strontium isotopes are fractionated in a diffusive boundary layer, however, the magnitude of this fractionation is not clear.

In solutions with very high $[Ca^{2+}]/[CO_3^{2-}]$ ratio, like in seawater or in our experiments, the limited supply of CO_3^{2-} ions for precipitation of calcite prevents the development of a strong diffusional $[Ca^{2+}]$ gradient (DePaolo, 2011; see Appendix). On the other hand, Fantle and DePaolo (2007) suggested that the enrichment of heavy calcium isotopes in a diffusive boundary layer around fast growing calcite crystals could explain results of Lemarchand et al. (2004). The latter observed an increase in $\delta^{44/40}Ca$ of calcite with increasing precipitation rate, opposite to the later observations of Tang et al. (2008b). Originally, Lemarchand et al. (2004) had explained this observation by the entrapment of an increasing percentage of unfractionated dissolved Ca^{2+} at very fast crystal growth rates. Much lower $\delta^{44/40}Ca$ values at low growth rates were explained by partial isotopic equilibration between fluid and crystal. Lemarchand et al. (2004) consequently estimated the equilibrium $^{44}Ca/^{40}Ca$ fractionation of calcite ($\Delta^{44/40}Ca_{eq(carb-aq)}$) as on the order of -1.5‰. In a study of the isotopic composition of pore fluids in Neogene calcite oozes from the Ontong Java Plateau Fantle and DePaolo (2007) showed that calcium isotope equilibrium fractionation should in fact lead to high $\delta^{44/40}Ca$ values, thereby disproving the model of Lemarchand et al. (2004). Additional evidence for the boundary layer model of Fantle and DePaolo (2007) was provided by the strongly reduced isotope fractionation in experiments by Lemarchand et al. (2004) where the growth solution was stirred, while much stronger fractionation effects were found in unstirred experiments. Neither Lemarchand et al. (2004) nor Fantle and DePaolo (2007) attempted to quantify the fractionation processes in the diffusive boundary layer. New experimental and theoretical results (Bourg et al., 2010; Watson and Müller, 2009) have recently provided the basis for a quantification

of such processes. We therefore developed a set of equations based on the diffusion model of Watson and Müller (2009) and the measurements of diffusive calcium isotope fractionation in water (Bourg et al., 2010) to quantify the isotope fractionation in diffusive boundary layers. We use a simplified 1-dimensional steady state approach (Watson and Müller, 2009). This approach provides an upper limit for possible isotope fractionation effects, because the latter are maximized for 1-dimensional diffusion and for steady state (i. e. for a constant concentration gradient in the diffusive boundary layer).

To calculate isotope fractionation effects in the diffusive boundary layer we use three equations describing the composition of the DBL at the liquid-crystal boundary (see Appendix for derivation of the equations). The solute concentrations of the major calcite constitutents, Ca^{2+} and CO_3^{2-}, are described by Eq. (8):

$$C_L = (C_0 * D - V * BT * C_X) / (D - V * BT) \qquad (8)$$

C_L (C^{Ca}_L, C^{CO3}_L) is the ion concentration at the liquid-crystal boundary (mmol/cm³). V is the crystal extension rate (cm/s), which is related to precipitation rate, R, by $V = R * M_{cc} / \rho_{cc}$, with the molecular weight ($M_{cc} = 100.0869$ g/mol) and the density ($\rho_{cc} = 2.71$ g/cm³) of calcite. BT is the boundary layer thickness (cm). D is the diffusion coefficient ($D_{Ca} = 7*10^{-6}$ cm²/s, Boudreau, 1997, $D_{CO3} = 8*10^{-6}$ cm²/s, Wolf-Gladrow and Riebesell, 1997). C_x and C_0 are the concentrations in the calcite crystal and in the bulk fluid, respectively ($C^{Ca}_x = C^{CO3}_x = 27.1$ mmol/cm³, $C^{Ca}_0 = 10.3$ μmol/cm³, $C^{CO3}_0 = 0.26$ μmol/cm³; with C^{CO3}_0 for warm ocean surface waters).

The latter numbers show that concentrations increase by several orders of magnitude between bulk fluid and calcite crystal. Therefore high precipitation rates can only be maintained if very thin boundary layers allow a sufficiently fast diffusive transport of the rate limiting ions, i.e. of CO_3^{2-} in seawater-like solutions. The maximum rates in our experiments ($10^{4.2}$ μmol/m²/h) can only be maintained with a boundary layer thickness of less than about 0.05-0.1 mm (see Appendix, Table A2).

The difference in the calcium isotopic composition between bulk fluid and the fluid at the liquid-crystal interface is given by:

$$\Delta^{44/40}Ca_{DBL} = (C^{Ca}_0 * \alpha^{44}_d * D_{Ca} / (V * BT * (\alpha^{44}_x * C^{Ca}_X - C^{Ca}_L) + \alpha^{44}_d * D_{Ca} * C^{Ca}_L) -1) * 1000 \qquad (9)$$

C^{Ca}_L is calculated with Equ. (8). There are two different isotope fractionation processes that modify

the composition of the diffusive boundary layer. One is reflected in the fractionation factor α^{44}_d which describes the $^{44}Ca/^{40}Ca$ fractionation during diffusive transport of calcium in water, D^{44}_{Ca}/D^{40}_{Ca}. Bourg et al. (2010) determined $\alpha^{44}_d = 0.99957$. The faster diffusive transport of light calcium leads to an enrichment of light isotopes in the boundary layer compared to the bulk fluid. The second mechanism changing the isotopic composition in the DBL is the preferential uptake of light calcium by the calcite crystal, reflected in α^{44}_x. For room temperature α^{44}_x was estimated to be about 0.9985 (-1.5‰) by Lemarchand et al. (2004), in general agreement with the DePaolo (2011) model results (-1.6 to -1.7‰) and with our experimental results (-1.6‰, see Fig. 3). A lower value for α^{44}_x (0.9980, -2.0‰) was reported by Reynard et al. (2011). We use 0.9985 in Eq. (9) which results in a maximum $\Delta^{44/40}Ca_{DBL}$ of 1.07‰ with the unrealistic assumption that calcium can be completely depleted at the liquid-crystal boundary, or more realistically, 0.05‰ if calcium depletion is limited by carbonate ion availability as discussed above (Figure 4; see also Appendix). With the lower α^{44}_x value of Reynard et al. (2011) the maximum $\Delta^{44/40}Ca_{DBL}$ would increase to 1.57 or 0.07‰, respectively. In any case, the heavy isotope enrichment effect of α^{44}_x dominates over the diffusive depletion, α^{44}_d. Therefore $\Delta^{44/40}Ca_{DBL}$ is always positive. It increases with increasing crystal growth rate (Fig. 4) and with increasing boundary layer thickness (Table A1). This can be different for DBLs in media where α^{44}_d is smaller than α^{44}_x, e.g. in hot silicate melts (Richter et al. 2003).

In general $\Delta^{44/40}Ca_{DBL}$ is a linear function of the relative depletion of calcium in the DBL, C^{Ca}_L/C^{Ca}_0 (Fig. 5). At higher C^{Ca}_0 the relative depletion C^{Ca}_L is less strong for given V and BT values. Therefore the magnitude of $\Delta^{44/40}Ca_{DBL}$ decreases with increasing bulk calcium concentration C^{Ca}_0 (Fig. 4).

The DBL effect on strontium isotopes is quantified by

$$\Delta^{88/86}Sr_{DBL} = ((V * BT * \alpha^{88}_d * (K_d^{Sr} * C^{Ca}_X - C^{Ca}_L) + \alpha^{88}_d * D_{Sr} *C^{Ca}_L) /$$
$$(V * BT * (\alpha^{88}_x * K_d^{Sr} * C^{Ca}_X - C^{Ca}_L) + \alpha^{88}_d * D_{Sr} * C^{Ca}_L) -1) * 1000 \qquad (10)$$

K_d^{Sr} is the distribution coefficient of strontium between fluid and calcite. We use $K_d^{Sr} = 0.11$, the average from Table 1. D_{Sr}, the diffusion coefficient for Sr^{2+} in water, is very similar to that of Ca^{2+} (Li and Gregory, 1974). We therefore use the same coefficient for calcium and strontium. Assuming that isotope fractionation during diffusion of Sr^{2+} and Ca^{2+} depends primarily on the different isotope masses, as discussed in the previous section, we estimate $\alpha^{88}_d = D_{88Sr}/D_{86Sr}$ to be 0.99990 (-0.1‰), analogous to D_{44Ca}/D_{40Ca}. For α^{88}_x we use a value of 0.9997 (-0.3‰), which corresponds to the lowest $\Delta^{88/86}Sr_{carb-aq}$ value observed in our experiments (Fig. 3).

The uptake of strontium into calcite changes with the fluid Sr/Ca ratio, controlled by K_d^{Sr}. Therefore $\Delta^{88/86}Sr_{DBL}$ is independent of the bulk fluid strontium concentration, C^{Sr}_0, but rather depends on C^{Ca}_0 and C^{Ca}_L (see Appendix, Table A1). With the weaker isotope fractionation of strontium the increase of $\Delta^{88/86}Sr_{DBL}$ with crystal growth rate is much smaller than for calcium, but there is still always an enrichment in heavy isotopes in the DBL (Fig. 4). The maximum isotope fractionation constrained by available calcium is 0.2‰ (Fig. 5). With the carbonate chemistry limitations the maximum $\Delta^{88/86}Sr_{DBL}$ value is 0.001‰. Contrary to the DBL isotope fractionation effect for Ca, $\Delta^{88/86}Sr_{DBL}$ shows a non-linear relationship to the element depletion in the DBL (C^{Sr}_L/C^{Sr}_0 and C^{Ca}_L/C^{Ca}_0). Therefore $\Delta^{88/86}Sr_{DBL}$ and $\Delta^{44/40}Ca_{DBL}$ are not linearly correlated (Fig. 5).

The magnitude of isotope fractionation due to diffusional transport is much too small (Fig. 4) to explain the increasing depletion of heavy isotopes with increasing precipitation rate observed by Tang et al. (2008b) and in this study (Fig. 1). Rather, the preferred uptake of light isotopes into calcite enriches the fluid near the crystal in heavy isotopes. In fluids with low $[Ca^{2+}]/[CO_3^{2-}]$ ratios and high precipitation rates this process may lead to a significant fractionation effect with increasing heavy isotope enrichment at increasing precipitation rates. However, the DBL mechanism can not explain the positive $\Delta^{44/40}Ca_{carb-aq}$-rate relationship observed by Lemarchand et al. (2004) because $\Delta^{44/40}Ca_{DBL}$ differs significantly for experiments with different $[Ca^{2+}]$ concentrations. Lemarchand et al. (2004) observed no isotopic difference between experiments with $[Ca^{2+}]$ concentrations that differed by a factor of 10. As shown in Fig. 4 this concentration difference would have resulted in 10 times smaller $\Delta^{44/40}Ca_{DBL}$ values for the high concentrations. In well stirred experiments using fluids with seawater-like $[Ca^{2+}]/[CO_3^{2-}]$ ratios DBL effects are negligible for strontium and calcium isotopes (Fig. 4). We therefore conclude that diffusive boundary layer effects can not explain any of the rate dependencies of calcium and strontium isotope fractionation observed by Lemarchand et al. (2004), Tang et al. (2008b), and in this study.

4.3. Planktic foraminifera

Mg/Ca ratios of *G. ruber* specimens from the same core samples as used in this study inidcate a ~4°C temperature increase from the last glacial to the Holocene (Table 3). Two studies have previously observed a temperature dependence of strontium isotope fractionation in inorganic and biogenic aragonite (Fietzke and Eisenhauer, 2006; Rüggeberg et al., 2008). Applying the temperature sensitivities reported in these papers would result in a $\delta^{88/86}Sr$ difference of 0.02 to 0.13‰ between the glacial and Holocene *G. ruber* samples. The observed difference

(0.007±0.014‰; Table 3) does not indicate a temperature sensitivity of this magnitude for *G. ruber*. The measured mean foraminiferal $\Delta^{88/86}Sr_{carb-aq}$ value of -0.25‰ is significantly lower than most published values of marine biogenic carbonates where $\Delta^{88/86}Sr_{carb-aq}$ ranges from -0.20‰ to -0.12‰ (Krabbenhöft et al., 2010, Liebetrau et al., 2009; Ohno and Hirata, 2007). This means that planktic foraminifera shells are more strongly fractionated in $^{88}Sr/^{86}Sr$ than most other biogenic carbonates. On the other hand, the observed foraminiferal $\Delta^{88/86}Sr_{carb-aq}$ is in good agreement with the $\Delta^{88/86}Sr_{carb-aq}$ of inorganic calcite that is formed at high precipitation rate. We therefore suggest that the strong foraminiferal strontium isotope fractionation is caused by high precipitation rates (R>$10^{3.5}$ µmol/m²/h). Kisakürek et al. (2011) suggested similar fast precipitation rates to explain high Sr/Ca ratios and low calcium isotope values observed in cultured planktic foraminifera (*G. ruber* and *Globigerinella siphonifera*). Their model further suggested that shell formation used less than 50% of the calcium ions supplied to the calcification site. As we will show below, the foraminiferal strontium isotope fractionation data as well as the elemental Sr/Ca ratios and the calcium isotope fractionation are all compatible with calcite growth in a calcification space that is largely open to exchange with seawater, in accordance with the model of Kisakürek et al. (2011).

Our measured foraminiferal $\Delta^{88/86}Sr_{carb-aq}$ data, combined with published average values for K_d^{Sr} and $\Delta^{44/40}Ca_{carb-aq}$, plot close to the respective inorganic calcite regression lines (Fig. 2, 3). For this comparison we use the average $\Delta^{44/40}Ca_{carb-aq}$ = -1.14 ± 0.05‰ of *G. ruber* from culture experiments carried out at 27 to 30°C, pH of 8.3 to 8.4, 35 psu (Kisakürek et al., 2011). For *G. sacculifer* we use the average $\Delta^{44/40}Ca_{carb-aq}$ = -1.10 ± 0.09‰ of culture and sediment trap samples, representing specimens not showing strong temperature effects, and grown at different salinities and 27-28°C (Gussone et al., 2009; Griffith et al., 2008b). We further use average K_d^{Sr} values from a core top transect published by Elderfield et al. (2000). They found K_d^{Sr} values of 0.167 and 0.163 for *G. ruber* and *G. sacculifer*, respectively. As shown in Fig. 2, both foraminifera species plot within the 95%-confidence belt of the inorganic calcite regression line. This result indicates that both the strontium concentration and the isotopic composition of *G. ruber* and *G. sacculifer* can be explained by inorganic processes dominated by precipitation rate effects.

Consequently, we can use the regression in Fig. 1 to estimate the average precipitation rates of *G. ruber* and *G. sacculifer*. We find rates higher than $10^{3.5}$ µmol/m²/h, with a best fit value of $10^{3.9}$ µmol/m²/h for both species. Slightly lower precipitation rates of $10^{3.30}$ to $10^{3.48}$ µmol/m²/h were measured by Lea et al. (1995) using ^{48}Ca uptake experiments with the planktic foraminiferal species *Orbulina universa*. Using K_d^{Sr} to estimate precipitation rates, applying a regression of the data from Tang et al. (2008a), results in higher rates. We find a minimum rate of $10^{4.0}$ µmol/m²/h and a best fit

value of $10^{4.2}$ μmol/m^2/h.

The calcium isotopic composition of the two species shows slightly higher $\Delta^{44/40}Ca_{carb-aq}$ values than expected from the inorganic calcite data (Fig. 3), plotting just outside the 95% confidence belt. We assume that both the strontium concentration and the strontium isotopic composition of *G. ruber* and *G. sacculifer* are primarily explained by high precipitation rates (Fig. 2). In contrast, the calcium isotopic composition may be affected by an additional, albeit minor, mechanism.

As previously suggested, calcium isotopes in these planktic foraminifera are possibly influenced by a Rayleigh distillation effect (Griffith et al., 2008b; see discussion in Kisakürek et al., 2011). Rayleigh distillation can sufficiently explain the observed slight enrichment in $\delta^{44/40}Ca$. From the difference between the measured $\Delta^{44/40}Ca_{carb-aq}$ of -1.1‰ for *G. sacculifer* and *G. ruber* and the expected inorganic value from the $\Delta^{88/86}Sr_{carb-aq}$ - $\Delta^{44/40}Ca_{carb-aq}$ regression shown in Fig. 3, we can estimate the percentage of calcium in the calcification reservoir that is consumed during calcification. To do this, we take the $\delta^{44/40}Ca$ enrichment with respect to the 95% confidence belt of the regression in Fig. 3 and apply a Rayleigh fractionation equation (Zeebe and Wolf-Gladrow, 2001). For the given $\Delta^{88/86}Sr_{carb-aq}$ = -0.25‰ value of *G. sacculifer* and *G. ruber* we calculate that 20% to 50% of the calcium in the reservoir is used to form calcite with the measured apparent $\Delta^{44/40}Ca_{carb-aq}$. The most likely value is 30%.

The resulting Rayleigh effect on the apparent $K_d{}^{Sr}$ would be an increase by 0.025. The true $K_d{}^{Sr}$ would therefore be slightly lower than the measured value, but would still plot within the 95% confidence belt of the inorganic calcite line (Fig. 2). The true planktic foraminiferal $\Delta^{44/40}Ca_{carb-aq}$ value defined by the measured strontium isotope value and the regression line in Fig. 3 would be -1.3‰. This value corresponds to a calcification rate of $10^{3.8}$ μmol/m^2/h according to Tang et al. (2008b).

For the calculations outlined above we assume that all calcium is derived from a reservoir with seawater isotopic composition. In contrast, Griffith et al. (2008b) and Gussone et al. (2009) proposed models for calcification of planktic foraminifera which assumed a calcification reservoir that was depleted in ^{44}Ca with respect to seawater. Griffith et al. (2008b) further assumed a very efficient use of the calcium reservoir (85% Ca^{2+} used, in accord with Elderfield et al., 1996). Gussone et al. (2009) proposed a temperature-dependent utilization of a strongly fractionated internal calcium reservoir with admixture of seawater calcium to explain the strong temperature dependence of calcium isotope fractionation sometimes observed in *G. sacculifer.*

Our strontium isotope data cannot exclude these models of highly efficient utilisation of a ^{44}Ca depleted reservoir. Because very little strontium is taken up into foraminiferal calcite the

corresponding Rayleigh effect on $\Delta^{88/86}Sr_{carb-aq}$ is very small even if 85% of the calcium reservoir are used. With a calcification fluid of normal seawater composition (Sr/Ca$_{fluid}$ ca. 10 mmol/mol) and with a K_d^{Sr} of about 0.16 the percentage of Sr^{2+} used is 5% for 30% Ca^{2+} utilization and 25% for 85% Ca^{2+} utilization. The resulting Rayleigh effect on the apparent $\delta^{88/86}Sr$ would only be +0.005‰ and +0.030‰, respectively.

Consequently, while strontium isotopes provide a good proxy for the calcification rate of foraminiferal calcite, they do not provide useful constraints to quantify Rayleigh distillation effects. Nevertheless, our model is able to explain strontium incorporation, strontium isotope fractionation as well as calcium isotope fractionation in *G. sacculifer* and *G. ruber* calcite by very high precipitation rates (about $10^{3.8}$ µmol/m^2/h) from a fluid with seawater composition for both strontium and calcium, and a poor utilization efficiency for calcium (30% of available Ca^{2+}) and strontium (5% of available Sr^{2+}).

5. CONCLUSIONS

Strontium isotope fractionation of inorganic calcite is predominantly controlled by the precipitation rate with increasing fractionation at higher rates and no significant isotope fractionation at very low rates. This kinetic fractionation behaviour is similar for strontium and calcium isotopes, leading to a linear correlation of the two isotope systems in experimental inorganic calcites. The correlation indicates that a similar mechanism controls calcium and strontium isotope fractionation. This mechanism probably involves chemical kinetic fractionation of the hydrated cations (preferred desolvation of the isotopically light cations). In addition, strontium and calcium isotope partitioning are both inversely correlated with the rate dependent partitioning of strontium ions between fluid and calcite. Two different possible mechanisms that can explain this correlated behaviour of elemental and isotopic partitioning have been proposed in the Surface Entrapment Model (Watson, 2004; Tang et al., 2008 a,b) and recently in the Surface Kinetic Model of DePaolo (2011). This correlation can, however, not be explained by partitioning in a diffusive boundary layer around the growing calcite crystals.

The predominance of heavy isotope enrichment in the boundary layer over depletion by diffusional kinetic fractionation would lead to an enrichment of heavy isotopes in the crystal at increasing precipitation rates. The opposite was observed in our experiments for both calcium and strontium isotopes. Additionally, the relative enrichment of strontium with respect to calcium in the diffusive boundary layer would lead to a positive correlation of Sr/Ca ratios with both isotope systems. The opposite is observed in our experimental results. On the other hand, our observations do not exclude

either the Surface Entrapment Model or the Surface Kinetic Model. Both models can well explain the observed trends and correlations of elemental and isotope partitioning.

The exceptionally strong strontium isotope fractionation of planktic foraminifera can be explained by very fast precipitation of their calcitic chambers. Together with calcium isotope and Sr/Ca data from the two investigated species (*G. ruber, G. sacculifer*) the strontium isotope data point to calcification in a system where only a relatively small percentage of the calcium transported to the site of calcification is used for the formation of calcite.

ACKNOWLEGDEMENTS

REFERENCES

Al-Horani F. A., Al-Moghrabi S. M., de Beer D. (2003) The mechanism of calcification and its relation to photosynthesis and respiration in the scleractinian coral Galaxea fascicularis. *Marine Biology* **142**, 419-426.

Bigeleisen J. (1949) The Relative Reaction Velocities of Isotopic Molecules. *Journal of Chemical Physics* **17**, 675-678.

Böhm F., Gussone N., Eisenhauer A., Dullo W.-C., Reynaud S., Paytan A. (2006) Calcium isotope fractionation in modern scleractinian corals. *Geochimica et Cosmochimica Acta* **70**, 4452-4462.

Böhm F., Eisenhauer A., Rausch S., Bach W., Klügel A. (2009): Calcium isotope systematics of low temperature alteration carbonates in the ocean crust. Abstract 19th V.M. Goldschmidt Conference, Geochim. Cosmochim. Acta **73**/13 Suppl.1, A133.

Boudreau B. P. (1997) Diagenetic models and their implementation. 414 pp, Springer, Berlin.

Bourg I. C., Richter F. M., Christensen J. N., Sposito G. (2010) Isotopic mass dependence of metal cation diffusion coefficients in liquid water. *Geochimica et Cosmochimica Acta* **74**, 2249-2256.

Carpenter S. J., Lohmann K. C. (1992): Sr/Mg ratios of modern marine calcite: Empirical indicators of ocean chemistry and precipitation rate. Geochim. Cosmochim. Acta **56**, 1837-1849.

Coggon R. M., Teagle D. A. H., Smith-Duque C. E., Alt J. C., Cooper M. J. (2010) Reconstructing past seawater Mg/Ca and Sr/Ca from mid-ocean ridge flank calcium carbonate veins. *Science* **327**, 1114-1147.

de Beer D., Bissett A., de Wit R., Jonkers H. (2008) A microsensor for carbonate ions suitable for microprofiling in freshwater and saline environments. *Limnology and Oceanography: Methods* **6**, 532-541.

DePaolo D. J. (2004) Calcium Isotopic Variations Produced by Biological, Kinetic, Radiogenic and Nucleosynthetic Processes. *Reviews in Mineralogy and Geochemistry* **55**, 255-288.

DePaolo D. J. (2011) Surface kinetic model for isotopic and trace element fractionation during precipitation of calcite from aqueous solutions. *Geochimica et Cosmochimica Acta* **75**, 1039-1056.

de Souza G. F., Reynolds B. C., Kiczka M., Bourdon B. (2010) Evidence for mass-dependent isotopic fractionation of strontium in a glaciated granitic watershed. *Geochimica et Cosmochimica Acta* **74**, 2596-2614.

de Villiers S. (1999) Seawater strontium and Sr/Ca variability in the Atlantic and Pacific oceans. *Earth and Planetary Science Letters* **171**, 623-634.

Dietzel M., Usdowski E. (1996) Coprecipitation of Ni^{2+}, Co^{2+}, and Mn^{2+} with galena and covellite, and of Sr^{2+} with calcite during crystallization via diffusion of H_2S and CO_2 through polyethylene at 20°C: Power law and Nernst law control of trace element partitioning. *Chemical Geology* **131**, 55-65.

Dietzel M., Gussone N., Eisenhauer A. (2004) Co-precipitation of Sr^{2+} and Ba^{2+} with aragonite by membrane diffusion of CO_2 between 10 and 50 °C. *Chemical Geology* **203**, 139-151.

Elderfield H., Bertram C. J., Erez J. (1996) A biomineralization model for the incorporation of trace elements into foraminiferal calcium carbonate. *Earth and Planetary Science Letters* **142**, 409-423.

Elderfield H., Cooper M., Ganssen G. (2000) Sr/Ca in multiple species of planktonic foraminifera: Implications for reconstructions of seawater Sr/Ca. *Geochemistry Geophysics Geosystems* **1**. doi:10.1029/1999GC000031.

Fantle M. S., DePaolo D. J. (2006) Sr isotopes and pore fluid chemistry in carbonate sediment of the Ontong Java Plateau: Calcite recrystallization rates and evidence for a rapid rise in seawater

Mg over the last 10 million years. *Geochimica et Cosmochimica Acta* **70**, 3883-3904.

Fantle M. S., DePaolo D. J. (2007) Ca isotopes in carbonate sediment and pore fluid from ODP Site 807A: The $Ca^{2+}_{(aq)}$–calcite equilibrium fractionation factor and calcite recrystallization rates in Pleistocene sediments. *Geochimica et Cosmochimica Acta* **71**, 2524-2546.

Fietzke J., Eisenhauer A. (2006) Determination of temperature-dependent stable strontium isotope ($^{88}Sr/^{86}Sr$) fractionation via bracketing standard MC-ICP-MS. *Geochemistry Geophysics Geosystems* **7.** doi:10.1029/2006GC001243.

Friedman I., O'Neil J. R. (1977) Compilation of Stable Isotope Fractionation Factors of Geochemical Interest. *Geol. Surv. Prof. Pap*. 440–KK. US Govt. Printing Office.

Gradstein F., Ogg J., Smith A.(2004) A Geologic Time Scale 2004. 589p, Cambridge University Press, Cambridge.

Griffith E. M., Paytan A., Caldeira K., Bullen T. D., Thomas E. (2008a) A dynamic marine calcium cycle during the past 28 million years. *Science* **322**, 1671-1674.

Griffith E. M., Paytan A., Kozdon R., Eisenhauer A., Ravelo A. C. (2008b) Influences on the fractionation of calcium isotopes in planktonic foraminifera. *Earth and Planetary Science Letters* **268**, 124-136.

Gussone N., Eisenhauer A., Heuser A., Dietzel M., Bock B., Böhm F., Spero H. J., Lea D. W., Bijma J., Nägler T. F. (2003) Model for kinetic effects on calcium isotope fractionation ($\delta^{44}Ca$) in inorganic aragonite and cultured planktonic foraminifera. *Geochimica et Cosmochimica Acta* **67**, 1375-1382.

Gussone N., Böhm F., Eisenhauer A., Dietzel M., Heuser A., Teichert B. M. A., Reitner J., Wörheide G., Dullo W.-C. (2005) Calcium isotope fractionation in calcite and aragonite. *Geochimica et Cosmochimica Acta* **69**, 4485-4494.

Gussone N., Langer G., Thoms S., Nehrke G., Eisenhauer A., Riebesell U., Wefer G. (2006) Cellular calcium pathways and isotope fractionation in *Emiliania huxleyi. Geology* **34**, 625-628.

Gussone N., Langer G., Geisen M., Steel B. A., Riebesell U. (2007) Calcium isotope fractionation in coccoliths of cultured *Calcidiscus leptoporus, Helicosphaera carteri, Syracosphaera pulchra* and *Umbilicosphaera foliosa. Earth and Planetary Science Letters* **260**, 505-515.

Gussone N., Hönisch B., Heuser A., Eisenhauer A., Spindler M., Hemleben C. (2009) A critical evaluation of calcium isotope ratios in tests of planktonic foraminifers. *Geochimica et Cosmochimica Acta* **73**, 7241-7255.

Halicz L., Segal I., Fruchter N., Stein M., Lazar B. (2008) Strontium stable isotopes fractionate in the soil environments? *Earth and Planetary Science Letters* **272**, 406-411.

Jacobson A. D., Holmden C. (2008) $\delta^{44}Ca$ evolution in a carbonate aquifer and its bearing on the

equilibrium isotope fractionation factor for calcite. *Earth and Planetary Science Letters* **270**, 349-353.

Kerisit S., Parker S. C. (2004) Free energy of adsorption of water and metal ions on the [1014] calcite surface. *Journal of the American Chemical Society* **126**, 10152-10161.

Kisakürek B., Eisenhauer A., Böhm F., Hathorne E. C., Erez J. (2011) Controls on Calcium Isotope Fractionation in Cultured Planktic Foraminifera, *Globigerinoides ruber* and *Globigerinella siphonifera*. *Geochimica et Cosmochimica Acta* **75**, 427-443.

Knudson K. J., Williams H. M., Buikstra J. E., Tomczak P. D., Gordon G. W., Anbar A. D. (2010) Introducing $\delta^{88/86}$Sr analysis in archaeology: a demonstration of the utility of strontium isotope fractionation in paleodietary studies. *Journal of Archaeological Science* **37**, 2352-2364.

Köhler-Rink S., Kühl M. (2005) The chemical microenvironment of the symbiotic planktonic foraminifer Orbulina universa. *Marine Biology Research* **1**, 68-78.

Krabbenhöft A., Fietzke J., Eisenhauer A., Liebetrau V., Böhm F., Vollstaedt H. (2009) Determination of radiogenic and stable strontium isotope ratios (^{87}Sr/^{86}Sr; $\delta^{88/86}$Sr) by thermal ionization mass spectrometry applying an ^{87}Sr/^{84}Sr double spike. *Journal of Analytical Atomic Spectrometry* **24**, 1267-1271.

Krabbenhöft A., Eisenhauer A., Böhm F., Vollstaedt H., Fietzke J., Liebetrau V., Augustin N., Peucker-Ehrenbrink B., Müller M. N., Horn C., Hansen B. T., Nolte N., Wallmann K. (2010) Constraining the marine strontium budget with natural strontium isotope fractionations (^{87}Sr/^{86}Sr*, $\delta^{88/86}$Sr) of carbonates, hydrothermal solutions and river waters. *Geochimica et Cosmochimica Acta* **74**, 4097-4109.

Lea D. W., Martin P. A., Chan D. A., Spero H. J. (1995) Calcium uptake and calcification rate in the planktonic foraminifer Orbulina universa. *The Journal of Foraminiferal Research* **25**, 14-23.

Lemarchand D., Wasserburg G., Papanastassiou D. (2004) Rate-controlled calcium isotope fractionation in synthetic calcite. *Geochimica et Cosmochimica Acta* **68**, 4665-4678.

Li Y.-H., Gregory S. (1974) Diffusion of ions in sea water and in deep-sea sediments. *Geochimica et Cosmochimica Acta* **38**, 703-714.

Liebetrau V., Eisenhauer A., Krabbenhöft A., Fietzke J., Böhm F., Rüggeberg A., Gürs K. (2009) New perspectives on the marine Sr-isotope record: $\delta^{88/86}$Sr, ^{87}Sr/^{86}Sr*, and $\delta^{44/40}$Ca signatures of aragonitic molluscs throughout the last 27 Ma. Geochim. Cosmochim. Acta **73**/13 Suppl.1, A762.

Marriott C. S., Henderson G. M., Belshaw N. S., Tudhope A.W. (2004) Temperature dependence of δ^7Li, δ^{44}Ca and Li/Ca during growth of calcium carbonate. *Earth and Planetary Science Letters* **222**, 615-624.

McArthur J. M., Howarth R. J. (2004) Strontium Isotope Stratigraphy. In: Gradstein F. M., Ogg J. G., Smith A. G. (eds.) A Geologic Time Scale, 96-105, Cambridge University Press, Cambridge.

McArthur J. M., Rio D., Massari F., Castradori D., Bailey T., Thirlwall M., Houghton S. (2006) A revised Pliocene record for marine-$^{87}Sr/^{86}Sr$ used to date an interglacial event recorded in the Cockburn Island Formation, Antarctic Peninsula. *Palaeogeography, Palaeoclimatology, Palaeoecology* **242**, 126-136.

Megyes T., Grósz T., Radnai T., Bakó I., Pálinkás G. (2004) Solvation of Calcium Ion in Polar Solvents: An X-ray Diffraction and ab Initio Study. *The Journal of Physical Chemistry A* **108**, 7261-7271.

Miles G. A., Howe R. C. (1977) Biostratigraphic summary, Leg 37, Deep Sea Drilling Project. *Initial Reports DSDP* **37**, 977-983.

Milliman J. D., Droxler A. W. (1996) Neritic and pelagic carbonate sedimentation in the marine environment: ignorance is not a bliss, Geologische Rundschau **85**, 496-504.

Nier A. O. (1938) The isotopic constitution of strontium, barium, bismuth, thallium and mercury. *Physical Review* **5**, 275–278.

Nürnberg D., Müller A., Schneider R. R. (2000) Paleo-sea surface temperature calculations in the equatorial east Atlantic from Mg/Ca ratios in planktic foraminifera: A comparison to sea surface temperature estimates from U37K', oxygen isotopes, and foraminiferal transfer function. *Paleoceanography* **15**, 124–134.

Nürnberg D., Schönfeld J., Dullo W.-Chr. Rühlemann C. (2003): RV Sonne Cruise Report SO 164 RASTA. *GEOMAR Report* **109**, 151p.

Ohno T., Hirata T. (2007) Simultaneous Determination of Mass-dependent Isotopic Fractionation and Radiogenic Isotope Variation of Strontium in Geochemical Samples by Multiple Collector-ICP-Mass Spectrometry. *Analytical Sciences* **23**, 1275-1280.

Raiteri P., Gale J. D., Quigley D., Rodger P. M. (2010) Derivation of an Accurate Force-Field for Simulating the Growth of Calcium Carbonate from Aqueous Solution: A New Model for the Calcite−Water Interface. *The Journal of Physical Chemistry C* **114**, 5997-6010.

Reynard L. M., Day C. C., Henderson G. M. (2011) Large fractionation of calcium isotopes during cave-analogue calcium carbonate growth. *Geochimica et Cosmochimica Acta* **75**, 3726-3740.

Richter F. M., Davis A. M., DePaolo D. J., Watson E. B. (2003) Isotope fractionation by chemical diffusion between molten basalt and rhyolite. *Geochimica et Cosmochimica Acta* **67**, 3905–3923.

Rüggeberg A., Fietzke J., Liebetrau V., Eisenhauer A., Dullo W.-C., Freiwald A. (2008) Stable strontium isotopes ($\delta^{88/86}Sr$) in cold-water corals — A new proxy for reconstruction of intermediate ocean water temperatures. *Earth and Planetary Science Letters* **269**, 570-575.

Schiebel F. (2002) Planktic foraminiferal sedimentation and the marine calcite budget. Global Biogeochemical Cycles **16**. doi:10.1029/2001GB001459.

Seward T. M., Henderson C. M. B., Charnock J. M., Driesner T. (1999) An EXAFS study of solvation and ion pairing in aqueous strontium solutions to 300°C. *Geochimica et Cosmochimica Acta* **63**, 2409-2418.

Steiger R. H., Jäger E. (1977) Subcommission on geochronology: convention on the use of decay constants in geochronology and cosmochronology. *Earth and Planetary Science Letters* **36**, 359-362.

Stevenson E. I., Burton K., Mokadem F., Parkinson I. J., Anand P., Hathorne E.C. (2010) The retrieval of marine weathering records preserved by strontium stable isotopes in foraminifera. *EOS Trans. AGU* **91** Fall Meeting Suppl., Abstract B21D-0343.

Tang J., Köhler S. J., Dietzel M. (2008a) Sr^{2+}/Ca^{2+} and $^{44}Ca/^{40}Ca$ fractionation during inorganic calcite formation: I. Sr incorporation. *Geochimica et Cosmochimica Acta* **72**, 3718-3732.

Tang J., Dietzel M., Böhm F., Köhler S. J., Eisenhauer A. (2008b) Sr^{2+}/Ca^{2+} and $^{44}Ca/^{40}Ca$ fractionation during inorganic calcite formation: II. Ca isotopes. *Geochimica et Cosmochimica Acta*, **72**: 3733-3745.

Tesoriero A. J., Pankow J. F. (1996) Solid solution partitioning of Sr^{2+}, Ba^{2+}, and Cd^{2+} to calcite. *Geochimica et Cosmochimica Acta* **60**, 1053-1063.

Tofteberg T., Öhrn A., Karlström G. (2006) Combined quantum chemical statistical mechanical simulations of Mg^{2+}, Ca^{2+} and Sr^{2+} in water. *Chemical Physics Letters* **429**, 436-439.

Watson E. B. (2004) A conceptual model for near-surface kinetic controls on the trace-element and stable isotope composition of abiogenic calcite crystals. *Geochimica et Cosmochimica Acta* **68**, 1473-1488.

Watson E. B., Müller T. (2009) Non-equilibrium isotopic and elemental fractionation during diffusion-controlled crystal growth under static and dynamic conditions. *Chemical Geology* **267**, 111-124.

Wolf-Gladrow D., Riebesell U. (1997) Diffusion and reactions in the vicinity of plankton: A refined model for inorganic carbon transport. *Marine Chemistry* **59**, 17-34.

Wombacher F., Eisenhauer A., Böhm F., Gussone N., Regenberg M., Dullo W.-C., Rüggeberg A. (2011) Magnesium stable isotope fractionation in marine biogenic calcite and aragonite. *Geochimica et Cosmochimica Acta* **75**, 5797-5878.

Young E. D., Galy A., Nagahara H. (2002) Kinetic and equilibrium mass-dependent isotope fractionation laws in nature and their geochemical and cosmochemical significance. *Geochimica et Cosmochimica Acta* **66**, 1095-1104.

Zeebe R. E., Wolf-Gladrow D. (2001) CO$_2$ in Seawater: Equilibrium, Kinetics, Isotopes. Elsevier Oceanography Series, 65, 346 p., Elsevier, Amsterdam.

FIGURE CAPTIONS

Fig. 1: Rate dependence of strontium isotope fractionation in experimental inorganic calcite. Precipitation rates are taken from Tang et al. (2008b). Dashed lines represent 95% confidence belts. Two samples of natural calcite that formed in ocean crust basalts with very low precipitation rates are shown for comparison, but not included in the regression. Precipitation rates for these two samples were estimated from the measured Sr/Ca ratios using the rate dependence from Tang et al. (2008a). The strontium isotope value measured for *G. ruber* and *G. sacculifer* is indicated by the arrow. Error bars represent average 2SEM of repeated sample measurements.

Fig. 2: Linear correlation of strontium isotope fractionation and the Sr/Ca distribution coefficient ($K_d{}^{Sr}$) in experimental inorganic calcite. Calcites from ocean crust basalts plot close to the extrapolated regression line. The values from planktic foraminifera plot within the 95% confidence belt (dashed lines). $K_d{}^{Sr}$ values of the foraminifera are from Elderfield et al. (2000) and represent average values of a range of core top samples ($K_d{}^{Sr} = 0.167$ for *G. ruber*, $K_d{}^{Sr} = 0.163$ for *G. sacculifer*). Error bars represent average 2SEM of repeated sample measurements.

Fig. 3: Linear correlation of strontium and calcium isotope fractionation in experimental inorganic calcite. Dashed lines represent 95% confidence belts. Calcites from ocean crust basalts plot close to the extrapolated regression line. Foraminiferal data show a slight enrichment of ^{44}Ca compared to the value expected from the inorganic regression. The calcium isotope values are averages, with $\Delta^{44/40}Ca_{carb-aq} = -1.14‰$ for cultured *G. ruber*, experiments at 27-30°C, 35 psu, pH of 8.3 to 8.4, $\delta^{44/40}Ca$ of seawater $=1.84‰$ (SRM915a) from Kisakürek et al. (2011); $\Delta^{44/40}Ca_{carb-aq} = -1.10‰$ for *G. sacculifer* from culturing experiments and sediment trap samples, 27-28°C (Gussone et al., 2009; Griffith et al., 2008b). Error bars represent average 2SEM of repeated sample measurements.

Fig. 4: Model calculations of the steady state isotope fractionation between bulk fluid and the liquid-crystal boundary ($\Delta^{44/40}Ca_{DBL}$ and $\Delta^{88/86}Sr_{DBL}$) in a diffusive boundary layer of 50 µm width around a growing calcite crystal. Crystal growth rates include the typical range of experimental and biogenic calcite growth as indicated by the arrow. Calcite growth rates in seawater are limited by the availability of carbonate ions. The plotted range includes the highest possible rate in normal marine settings for BT=50 µm (see Appendix, Table A2). The strontium curve is calculated for normal seawater Ca^{2+} concentration. Calcium calculations are shown for seawater concentration and

26

ten times seawater concentration. The curves include the effects of diffusive isotope fractionation and depletion of the isotope species which is preferentially taken up into the crystal. The effect of diffusive fractionation (Bourg et al., 2010) is shown for comparison, calculated for a normal seawater Ca^{2+} concentration.

Fig. 5: Modelled correlation between strontium and calcium isotope fractionation due to diffusion and isotope depletion in a diffusive boundary layer adjacent to calcite crystals growing at rates between 10^2 and $10^{4.7}$ µmol/m^2/h, with boundary layer thicknesses ranging from 50 to 500 µm. Numbers above and below the graph indicate the Ca depletion (C^{Ca}_L/C^{Ca}_0) and Sr depletion (C^{Sr}_L/C^{Sr}_0) in the DBL, respectively. Note that in seawater the Ca depletion in the DBL is limited to C^{Ca}_L/C^{Ca}_0 values >0.95 by the availability of carbonate ions.

Table 1: Inorganic calcite precipitation experiments.

Experiment #	log(R) (μmol/m^2/h)	$\Delta^{44/40}Ca_{carb-aq}$ (‰)	f_{Ca}	$\Delta^{44/40}Ca_{RC}$ (‰)	K_d^{Sr}	Sr_{cc} (μg/g)	M_{cc} (mg)	SI_{cc}	$\Delta^{88/86}Sr_{carb-aq}$ (‰)	$^{87}Sr/^{86}Sr$
11 (C29)	4.21	-1.50±0.19	0.89	-1.59	0.16	1477	510	1.21	-0.292±0.034	0.707854
14 (C32)	3.02	-0.80±0.08	0.90	-0.84	0.09	830	480	0.94	-0.164±0.020	0.707852
15 (C34)	2.25	-0.62±0.16	0.85	-0.67	0.07	600	730	0.66	-0.153±0.002	0.707849
16 (C35)	3.34	-1.03±0.12	0.93	-1.07	0.11	932	370	0.89	-0.199±0.019	0.707836
17 (C37)	2.39	-0.51±0.01	0.94	-0.53	0.06	525	310	0.65	-0.086±0.002	0.708709
19 (C39)	4.18	-1.37±0.15	0.91	-1.43	0.17	1503	430	1.21	-0.263±0.012	0.708701

Experiment numbers, precipitation rates (log(R)), calcium isotope fractionation between fluid and calcite ($\Delta^{44/40}Ca_{carb-aq}$ with 2SEM errors), strontium distribution coefficients (K_d^{Sr}), strontium concentration in calcite (Sr_{cc}), total mass of calcite precipitated (M_{cc}), and the critical saturation index for the precipitation of calcite (SI_{cc}) are from Tang et al. (2008a,b). All experiments were carried out at 25°C, a pH of 8.3 and an ionic strength of about 0.035 M. Initial Ca^{2+} and Sr^{2+} concentrations in the precipitating fluid (5 L) were 9.9 mM and 95 μM, respectively. Rayleigh fractionation corrected calcium isotope values were calculated from the remaining Ca fraction in solution (f_{Ca}) using $\Delta^{44/40}Ca_{RC}$= (ln(f_{Ca} * $\Delta^{44/40}Ca_{carb-aq}$/1000 - $\Delta^{44/40}Ca_{carb-aq}$/1000 + f_{Ca}) / ln(f_{Ca}) - 1) *1000. Sr^{2+} consumption was less than 2% in all experiments, therefore no Rayleigh correction was applied. Strontium isotope fractionation ($\Delta^{88/86}Sr_{carb-aq}$ with 2SEM errors from repeated analyses, n=2 for all samples) is the difference between the measured calcite sample composition and the dissolved Sr^{2+} composition in the fluid, with $\delta^{88/86}Sr_{fluid}$ = 0.156 ± 0.005‰ (relative to SRM 987). Precision (1sd) is: log(R) ±0.12, K_d^{Sr} ±0.01, $^{87}Sr/^{86}Sr$ ±10^{-5}.

Table 2: Inorganic calcite cements from ocean crust basalt.

Core Interval	Basement Depth (m)	$\delta^{18}O$ (‰ VPDB)	T_{calc} (°C)	$^{87}Sr/^{86}Sr$	^{87}Sr Age (Ma)	Sr/Ca_{cc} (mmol/mol)	$\Delta^{44/40}Ca$ (‰)	$\Delta^{88/86}Sr$ (‰)
335-7-3, 105cm	17	3.22	2	0.70896	6.8±0.6	0.33	-0.17	-0.058
335-9-1, 50 cm	33	3.30	1	0.70897	6.5±0.5	0.30	-0.09	-0.049

Both cores are from DSDP Leg 37. Oxygen isotopes, $^{87}Sr/^{86}Sr$, Sr/Ca ratios in the calcite (Sr/Ca_{cc}), and calcium isotopes are from Böhm et al. (2009). T_{calc} is the calcite formation temperature calculated from $\delta^{18}O$ assuming a $\delta^{18}O$ of seawater of -0.5‰ (VSMOW) and applying the calibration of Friedman and O'Neil (1977). The ^{87}Sr ages were calculated from the measured $^{87}Sr/^{86}Sr$ ratios, adjusted to a $^{87}Sr/^{86}Sr_{SRM987}$ of 0.710248, by comparing with the Strontium Isotope Stratigraphy of McArthur and Howarth (2004). The $\Delta^{44/40}Ca$ value is the difference between the measured $\delta^{44/40}Ca$ of the calcite and seawater with an estimated $\delta^{44/40}Ca$ at the time of calcite formation (ca. 7 Ma) of 1.9±0.1‰ (SRM915a) (e.g. Griffith et al., 2008a). The $\Delta^{88/86}Sr$ values were calculated accordingly, assuming that seawater at 7 Ma had the same $\delta^{88/86}Sr$ as today (0.386‰ SRM987, Krabbenhöft et al., 2009). Analytical precision (1sd) is ±0.03‰ for $\delta^{18}O$, ±10^{-5} for $^{87}Sr/^{86}Sr$, ±0.01 mmol/mol for Sr/Ca_{cc}, ±0.1‰ for $\delta^{44/40}Ca$, and ±0.01‰ for $\delta^{88/86}Sr$.

Table 3: *Globigerionides ruber* and *Globigerinoides sacculifer* samples.

Sample	Depth (cm)	Age (ka)	T (°C)	$\Delta^{88/86}Sr_{carb-aq}$ (‰)	$^{87}Sr/^{86}Sr$
HFB9r	10	1.4	29.9	-0.242	0.709180
HFB8r	26	4.1	30.3	-0.256	0.709171
HFB7r	43	7.0	30.5	-0.243	0.709177
Average Holocene *G. ruber*				**-0.247**	**0.709176**
HFB2r	106	22	26.9	-0.247	0.709168
HFB1r	116	25	26.5	-0.254	0.709175
116rub	116	25	26.5	-0.261	0.709174
Average glacial *G. ruber*				**-0.254**	**0.709173**
HFB10s	10	1.4	27.0	-0.253	0.709185
10sacc	10	1.4	27.0	-0.259	0.709162
HFB11s	26	4.1	n.a.	-0.243	0.709171
HFB12s	43	7.0	26.6	-0.245	0.709159
43sacc	43	7.0	26.6	-0.242	0.709159
Average Holocene *G. sacculifer*				**-0.248**	**0.709167**

Temperatures were calculated from Mg/Ca ratios of specimens of the two species picked from the same samples using the temperature calibration of Nürnberg et al. (2000); depositional ages are based on oxygen isotope analyses of benthic foraminifera (C. Horn, doctoral thesis, University of Kiel). Analytical precision (1sd) is ±0.01‰ for $\delta^{88/86}Sr$, and ±10^{-5} for $^{87}Sr/^{86}Sr$. Standard error of the $\delta^{88/86}Sr$ mean values (2SEM) is ±0.009‰ for Holocene *G. ruber*, ±0.008‰ for glacial *G. ruber*, and ±0.006‰ for *G. sacculifer*. All $\Delta^{88/86}Sr_{carb-aq}$ values were calculated with a seawater $\delta^{88/86}Sr$ of 0.386±0.08‰ (Krabbenhöft et al., 2009).

Appendix

Derivation of steady state equations describing isotope and concentration effects in the diffusive boundary layer (DBL)

We derive steady state equations for the DBL concentrations and isotope ratios of Ca^{2+} and Sr^{2+} for calcite growing in aqueous solution. Our equations are based on Equations 6 and 7 of Watson and Müller (2009) which describe 1-dimensional steady state diffusion in a diffusive boundary layer. The two equations quantify the concentration of a solute at the liquid-crystal interface and are combined in Eq. (A1). The left hand side of Eq. (A1) describes the transport of ions from the fluid into the crystal. In steady state this flux is balanced by a diffusive flux from the bulk solution to the liquid-crystal interface (right hand side).

$$(C_L - C_X) * A * \delta t * V = A * \delta t * D (C_L - C_0) / BT \tag{A1}$$

C_L, C_0 and C_X are the concentrations of the ion of interest in the fluid of the liquid-crystal interface, in the bulk fluid, and in the crystal, respectively (in $mmol/cm^3$). For calcite growing in aqueous solution these can be the concentrations of Ca^{2+} or CO_3^{2-}. A is the growing surface area of the crystal (cm^2), δt is a short time increment (s), V is the radial crystal extension velocity (cm/s), D is the diffusion coefficient (cm^2/s), and BT is the thickness of the diffusive boundary layer (cm). Equation A1 can be solved for C_L, the solute concentration at the liquid-crystal interface:

$$C_L = (C_0 * D - V * BT * C_X) / (D - V * BT) \tag{A2}$$

The concentration of an isotope or a trace element substituting for a major ion (e.g. ^{44}Ca or Sr substituting for Ca in calcite) can be calculated with the same equation.

$$C^{44}_L = (C^{44}_0 * D^{44} - V * BT * C^{44}_X) / (D^{44} - V * BT) \tag{A3}$$

Equation (A3) can be rewritten using the following definitions

$D^{44} = \alpha^{44}_d * D_{Ca}$

$C^{44}_0 = C^{Ca}_0 * R^{44}_{fl}$

$C^{44}_x / C^{Ca}_x = \alpha^{44}_x * C^{44}_L / C^{Ca}_L$

where α^{44}_x is the ^{44}Ca/^{40}Ca isotope fractionation factor between fluid and crystal, α^{44}_d is the isotope fractionation during diffusive transport of ions, and R^{44}_{fl} is the molar fraction of ^{44}Ca relative to total Ca in the bulk fluid (C^{Ca}_0):

$$C^{44}_L = (R^{44}_{fl} * C^{Ca}_0 * \alpha^{44}_d * D_{Ca} - V * BT * \alpha^{44}_x * C^{Ca}_X * C^{44}_L/C^{Ca}_L) / (\alpha^{44}_d * D_{Ca} - V * BT)$$

$$\tag{A4}$$

Solving for C^{44}_L and dividing by C^{Ca}_L quantifies the molar fraction of ^{44}Ca at the liquid-crystal interface:

$$C^{44}_L / C^{Ca}_L = (R^{44}_{fl} * C^{Ca}_0 * \alpha^{44}_d * D_{Ca}) / (V * BT * (\alpha^{44}_x * C^{Ca}_X - C^{Ca}_L) + \alpha^{44}_d * D_{Ca} * C^{Ca}_L)$$

$$\tag{A5}$$

The isotope effect of the diffusive boundary layer can be described by the offset in the isotopic composition ($\delta^{44/40}Ca$) between the bulk fluid and the liquid-crystal interface as

$$\Delta^{44/40}Ca_{DBL} = \delta^{44/40}Ca_L - \delta^{44/40}Ca_0 \approx (C^{44}_L/C^{Ca}_L \ / \ R^{44}_{fl} - 1) * 1000 \tag{A6}$$

Equation (A6) is an approximation based on the assumption that $C^{40}_L/C^{40}_0 = C^{Ca}_L/C^{Ca}_0$, i.e. that the concentration gradient from bulk solution to the liquid-crystal boundary is very similar for total calcium and for ^{40}Ca. Because there is isotope fractionation in the DBL, the $^{44}Ca/^{40}Ca$ ratio and consequently the $^{40}Ca/Ca$ ratio are changed resulting in $C^{40}_L/C^{Ca}_L = x * C^{40}_0/C^{Ca}_0$, where x is the error introduced by the approximation. Neglecting other calcium isotopes, which account for only 0.97% of total calcium, we estimate $x = (R^{44/40}_{fl} + 1) \ / \ (\alpha_{DBL} * R^{44/40}_{fl} + 1)$ from the natural molar $^{44}Ca/^{40}Ca$ ratio, $R^{44/40}_{fl}$ and the $^{44}Ca/^{40}Ca$ fractionation in the DBL, α_{DBL}. For $\alpha_{DBL} = 1.001$ (1‰) and $R^{44/40}_{fl} \approx 0.02152$ we get $x = 0.99998$. That means C^{40}_L is 0.02 ‰ more depleted with respect to the bulk concentration (C^{40}_0) than total calcium. The $\Delta^{44/40}Ca_{DBL}$ value calculated with Eq. (A6) therefore slightly underestimates the true DBL isotope effect, but the error is negligible.

Combining Eqs. (A5) and (A6) results in

$$\Delta^{44/40}Ca_{DBL} = (C^{Ca}_0 * \alpha^{44}_d * D_{Ca} \ / \ (V * BT * (\alpha^{44}_x * C^{Ca}_X - C^{Ca}_L) + \alpha^{44}_d * D_{Ca} * C^{Ca}_L) - 1) * 1000 \tag{A7}$$

C^{Ca}_L can be calculated for a calcite crystal growing in aqueous solution using Eq. (A2) with given values of BT, V, C^{Ca}_0, α^{44}_d, α^{44}_x, D_{Ca}, and with the concentration of calcium in calcite (C^{Ca}_X) of 27.1 mmol/cm^3. This value can be assumed to be sufficiently invariant in pure calcite, where only trace amounts of Ca are substituted by other cations (e.g. Sr).

In analogy to Eq. (A3) we quantify the concentrations of total Sr and ^{88}Sr at the liquid-crystal interface of a calcite crystal in Eqs. (A8) and (A9), respectively:

$$C^{Sr}_L = (C^{Sr}_0 * D_{Sr} - V * BT * C^{Sr}_X) \ / \ (D_{Sr} - V * BT) \tag{A8}$$

where D_{Sr} is the diffusion coefficient of Sr, C^{Sr}_X and C^{Sr}_0 are the concentrations of Sr (mmol/cm^3) in the calcite crystal and in the bulk fluid, respectively. For ^{88}Sr we can write:

$$C^{88}_L = (C^{88}_0 * D_{88} - V * BT * C^{88}_X) \ / \ (D_{88} - V * BT) \tag{A9}$$

As for the calcium isotopes we can define:

$$D^{88} = \alpha^{88}_d * D_{Sr}$$

$$C^{88}_0 = C^{Sr}_0 * R^{88}_{fl}$$

$$C^{88}_X \ / \ C^{Sr}_X = \alpha^{88}_x * C^{88}_L \ / \ C^{Sr}_L$$

Where α^{88}_x and α^{88}_d are the $^{88}Sr/^{86}Sr$ fractionation factors for crystallisation and diffusion, respectively. With that Eq. (A9) can be rearranged, similar to Eq. (A5), to

$$C^{88}_L \ / \ C^{Sr}_L = (R^{88}_{fl} * C^{Sr}_0 * \alpha^{88}_d * D_{Sr}) \ / \ (V * BT * (\alpha^{88}_x * C^{Sr}_X - C^{Sr}_L) + \alpha^{88}_d * D_{Sr} * C^{Sr}_L) \tag{A10}$$

The concentration of Sr in calcite, C^{Sr}_X, depends on the Sr/Ca partition coefficient between calcite and solution:

$$K_d = C^{Sr}_X/C^{Ca}_X \ / \ C^{Sr}_L/C^{Ca}_L$$

With that Eq. (A8) can be rearranged to

$$C^{Sr}_L = C^{Ca}_L * D_{Sr} * C^{Sr}_0 / (V * BT * (K_d * C^{Ca}_X - C^{Ca}_L) + C^{Ca}_L * D_{Sr}) \qquad (A11)$$

Combining and rearranging Eqs. (A10) and (A11) in analogy to Eq. (A6) results in

$$\Delta^{88/86}Sr_{DBL} = ((V * BT * \alpha^{88}_d * (K_d * C^{Ca}_X - C^{Ca}_L) + \alpha^{88}_d * D_{Sr} *C^{Ca}_L) /$$

$$(V * BT * (\alpha^{88}_x * K_d * C^{Ca}_X - C^{Ca}_L) + \alpha^{88}_d * D_{Sr} * C^{Ca}_L) -1) * 1000 \qquad (A12)$$

The error of the approximation of $\Delta^{88/86}Sr_{DBL}$ by using total strontium instead of ^{86}Sr concentrations can be calculated analogous to Eq. (A6) with $R^{88/86}_{fl}= 0.119$. Again the calculated isotope offset underestimates the true DBL isotope effect. For $\alpha_{DBL}= 1.0002$ (0.2‰) the error amounts to 0.02 ‰.

Sensitivities to different control parameters

Sensitivities of the isotope fractionation effects to the different parameters differ for Ca and Sr. We calculated the response to doubling of BT, V, C^{Ca}_0, C^{Sr}_0, D_{Ca}, D_{Sr}, K_d, Δ^{Ca}_{cryst}, Δ^{Ca}_{diff}, Δ^{Sr}_{cryst}, and Δ^{Sr}_{diff}, where $\Delta_{cryst} = (\alpha_x - 1) *1000$, and $\Delta_{diff} = (\alpha_d - 1) *1000$. The effects on $\Delta^{44/40}Ca_{DBL}$ and $\Delta^{88/86}Sr_{DBL}$ are shown in Table A1.

While Ca isotope effects change almost linearly, Sr isotopes show a non-linear behaviour at high BT*V values, when C^{Ca}_L becomes small compared to C^{Ca}_0. This strongly increases the Sr/Ca ratio near the crystal surface and therefore increases the uptake of Sr into the calcite crystal. The non-linear behaviour of the Sr isotope fractionation effect is conspicuous in its response to doubling of D_{Ca} and K_d (Table A1).

The Ca isotope effects depend on the bulk solution calcium concentration (C^{Ca}_0). In contrast, the isotope effect for Sr is independent of the bulk Sr concentration (C^{Sr}_0), but is closely linked to the bulk Ca concentration (C^{Ca}_0).

The effect of isotope fractionation during diffusion is outweighed by the effect of selective uptake of light isotopes during crystal growth. The DBL is enriched in light isotopes as long as $\Delta_{cryst}<\Delta_{diff}$. The isotope effect of the DBL, Δ_{DBL}, becomes zero when $\Delta_{cryst} =\Delta_{diff}$. Only when $\Delta_{cryst}>\Delta_{diff}$ the DBL will get enriched in light isotopes.

For both isotope systems the crystal growth rate (V) and the thickness of the boundary layer (BT) are major controlling factors. While the growth rate was measured in our precipitation experiments, we did not measure BT. This introduces the most significant uncertainty to the quantification of the DBL effects.

Table A1: Sensitivities of DBL isotope effects on doubling of system parameters

Parameter	Standard value	Doubling parameter changes Δ_{DBL} by	
		$\Delta^{44/40}Ca_{DBL}$	$\Delta^{88/86}Sr_{DBL}$
BT	0.1 mm	2-fold	about 2-fold
V	10^{-9} cm/s	2-fold	about 2-fold
C^{Ca}_0	10.3 mmol/L	0.5-fold	about 0.5-fold
C^{Sr}_0	0.09 mmol/L	no change	no change
D_{Ca}	$7*10^{-6}$ cm^2/s	0.5-fold	1-fold to 0.5-fold
D_{Sr}	$7*10^{-6}$ cm^2/s	no change	0.5-fold
Δ^{Ca}_{cryst}	-1.50 ‰	2.4-fold	no change
Δ^{Ca}_{diff}	-0.43 ‰	0.6-fold	no change
Δ^{Sr}_{cryst}	-0.30 ‰	no change	2.5-fold
Δ^{Sr}_{diff}	-0.10 ‰	no change	0.5-fold
K_d	0.11	no change	2-fold to 1.1-fold

Limits for the DBL thickness (BT)

For a given crystal growth rate the thickness of the boundary layer is limited by the concentrations of the Ca^{2+} and CO_3^{2-} ions at the liquid-crystal interface. The interface solution must be oversaturated with respect to calcite ($\Omega_{cc}>1$), otherwise the crystal stops growing. We use Eq. (A2) to calculate the concentrations of the two ions for a given bulk solution chemistry and a given crystal growth rate. With that we can estimate a maximum thickness of the boundary layer that still allows diffusion to maintain calcite oversaturation at the liquid-crystal interface.

The calculations were carried out for a seawater-like fluid composition, i.e. $C^{Ca}_0 = 10.3$ mmol/L and $C^{CO3}_0 = 0.26$ mmol/L. The calcite solubility constant $K_{cc}= 0.43$ mM^2 for the determination of Ω_{cc} was calculated for normal salinity and a temperature of 25°C (Zeebe & Wolf-Gladrow 2001). We use $C^{Ca}_X= 27.1$ mmol/cm^3 and $C^{CO3}_X= 27.1$ mmol/cm^3. We assume that the boundary layer thickness is similar for Ca^{2+}, CO_3^{2-}, and HCO_3^-. The boundary layer thickness in a stirred solution is controlled by turbulences in the fluid and therefore has a constant thickness for all ions. For crystals smaller than the smallest turbulences the boundary layer thickness is largely defined by the V/D ratio and the crystal radius, r_x (Watson and Müller, 2009). As V and r_x are identical for Ca^{2+}, CO_3^{2-}, and HCO_3^- ions and D in aqueous solution differs only slightly between these ions ($D_{Ca} = 7*10^{-6}$ cm^2/s, $D_{CO3} = 8*10^{-6}$ cm^2/s, $D_{HCO3} = 1*10^{-5}$ cm^2/s, Wolf-Gladrow and Riebesell, 1997), our assumption is a reasonable approximation.

As not only CO_3^{2-} ions are involved in the calcite growth we used the diffusion-reaction model described in Zeebe & Wolf-Gladrow (2001) to calculate speciation and diffusion of all carbonate system components. The latter approach slightly relaxes the constraints on BT given by considering CO_3^{2-} concentration only. This is because diffusion and reaction of OH^-, CO_2, and HCO_3^- contribute additional CO_3^{2-} ions for calcite formation.

Considering only CO_3^{2-} with a concentration typical for warm surface seawater we calculate a maximum possible DBL reduction of C^{Ca}_L to 97% of C^{Ca}_0 (with $C^{Ca}_0 = 10.3$ mM). Considering the whole carbonate system (ΣCO_2) the maximum possible C^{Ca}_L reduction only slightly changes to 95% of C^{Ca}_0. With the standard fractionations and diffusion constants listed in Table A1 the resulting maximum $\Delta^{44/40}Ca_{DBL}$ and $\Delta^{88/86}Sr_{DBL}$ values are 0.05‰ and 0.001‰, respectively. The corresponding BT values and maximum precipitation rates are shown in Table A2.

Table A2: Maximum DBL thickness and growth rate for calcite precipitation limited by $CO_3^{2-}/\Sigma CO_2$ availability and calcite saturation state in seawater

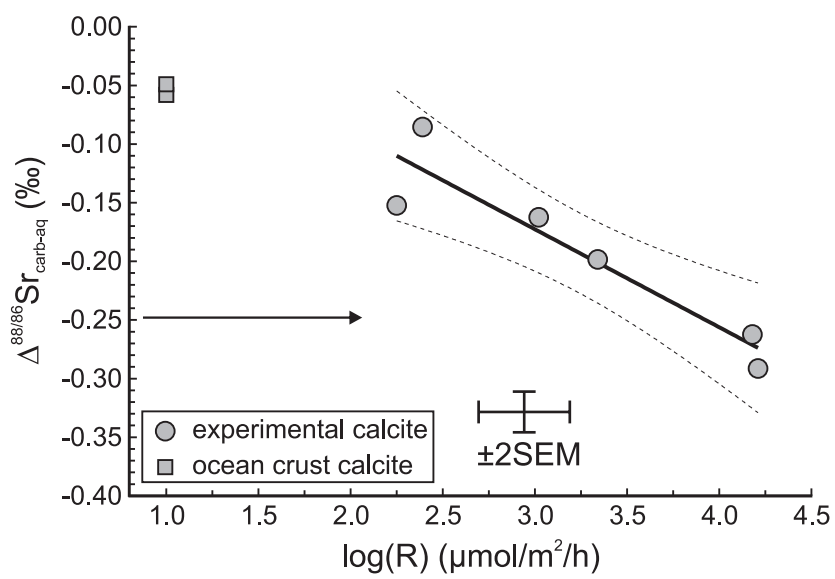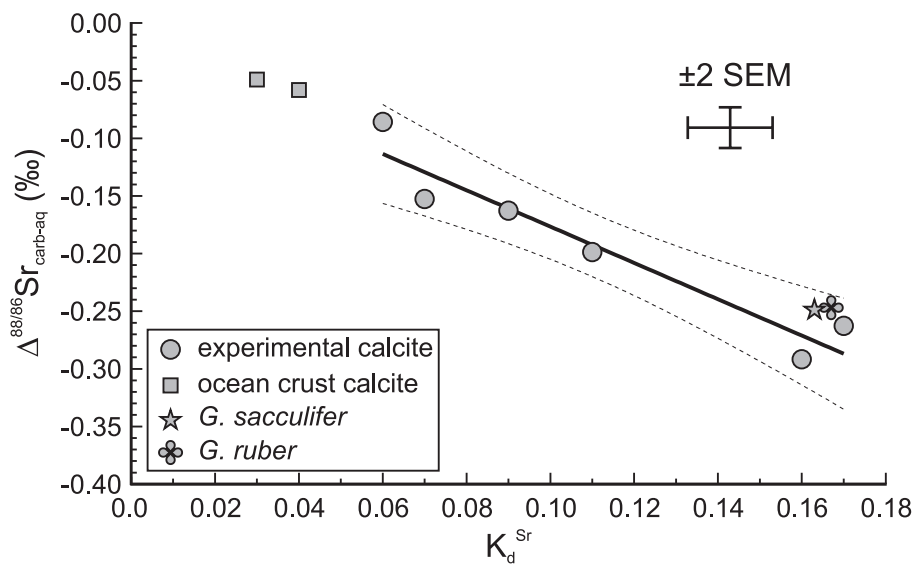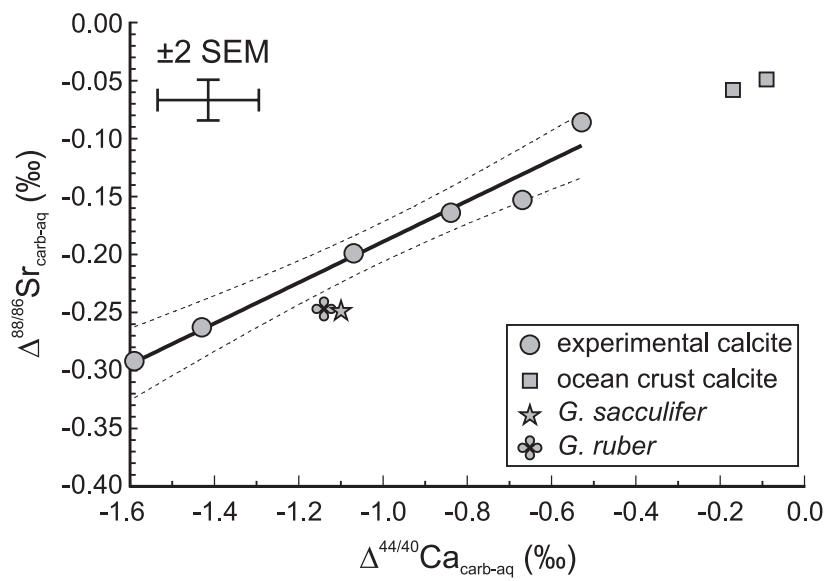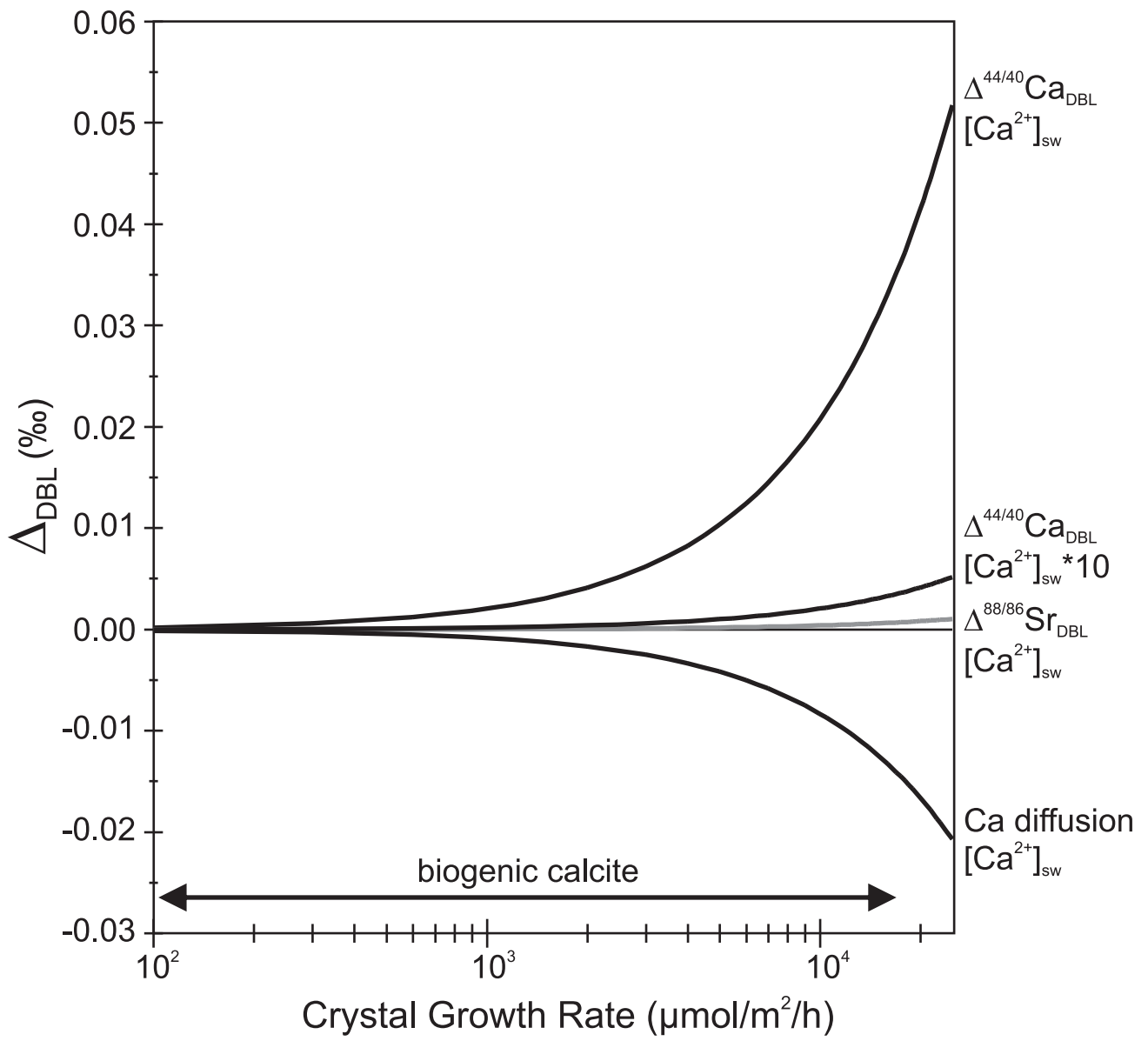| BT (mm)	maximum log(R) (μmol/m²/s)	
	CO_3^{2-} limited	ΣCO_2 limited
0.02	4.50	4.78
0.05	4.10	4.38
0.10	3.80	4.08
0.15	3.62	3.90
0.20	3.50	3.78
0.50	3.10	3.40
1.00	2.80	3.08
2.00	2.50	2.78

Fig. 1

Fig. 2

Fig. 3

Fig. 4

Fig. 5